Geophys. J. Int. (1993) **115,** 230–250

Scattering of elastic waves by a spherical inclusion—I. Theory and numerical results

Valeri A. Korneev and Lane R. Johnson

Department of Geology and Geophysics, and Center for Computational Seismology, Lawrence Berkeley Laboratory, University of California, Berkeley, California 94720, *USA*

Accepted 1993 March 8. Received 1993 March 1; in original form 1992 May 20

SUMMARY

A complete and exact solution for the problem of an incident *P* wave scattered by an elastic spherical inclusion is presented and described. The solution can be obtained from either analytical formulae or stable numerical procedures. A method of estimating the number of terms that must be retained in the harmonic series in order to achieve a specified accuracy is given. The results are investigated by calculating synthetic seismograms, scattering diagrams, and scattering cross-sections for a broad frequency band and for both low-velocity and high-velocity inclusions. The fields within the shadow zone are formed primarily from three different types of waves, *P* waves transmitted through the sphere, *P* waves diffracted around the sphere, and *S* waves converted at the boundary of the sphere. The relative contribution from these different waves depends upon the distance of the observation point from the sphere.

Key words: elastic waves, diffraction, scattering, sphere.

1 INTRODUCTION

The fact that the earth is not a homogeneous body has forced seismologists to consider scattered waves in their attempts to explain some of the features they observe on seismograms. Elastic wave scattering has been called upon to explain a variety of different phenomena which are routinely observed. These include the phase and amplitude fluctuations of waves arriving at a seismic array (Aki 1973), the precursors to *PKIKP* (Haddon & Cleary 1974), and the codas of local earthquakes (Aki 1969). In addition, the attenuation of seismic waves is usually interpreted as being a combination of intrinsic absorption and scattering (Aki 1980).

The general problem of scattering of elastic waves by a heterogeneity within the earth is a difficult one and analytical solutions are known for only a few special cases, and even in these instances the solutions are complicated and laborious to calculate. Thus, most attempts at interpreting scattered seismic waves have relied upon approximate treatments of the scattering theory. A number of approximations are possible and are related to such parameters as the size of the scatterer, the shape of the scatterer, the distance of the observation point from the scatterer, the magnitude of the heterogeneity, and the number of times the wave has been scattered. Assessing the validity of these approximations is not a simple matter and has been addressed for only some of the approximations (for example, Hudson & Heritage 1981). The matter is further complicated by the fact that more than one approximation may be involved in the same problem, and it is not always obvious that the different approximations are consistent.

The best method of checking the validity of the approximations which are made in scattering problems is to compare them with exact analytical solutions. In this paper we develop and discuss the properties of one such solution, the scattering of a plane *P* wave by a spherical inclusion. The method of obtaining the analytical solution is outlined, the numerical methods used in calculating the solution are described, and some of the important features of the solution are described and discussed. The results contained in this paper are the starting point for a companion paper (Korneev & Johnson 1993), which makes detailed comparisons between various approximations and the exact solution.

In setting up the theoretical problem for elastic wave scattering, one must choose a model which is complicated enough so that it resembles situations found in the earth and at the same time simple enough to allow tractable solutions of the mathematical equations. We have chosen to model a local heterogeneity as a homogeneous elastic sphere surrounded by a

homogeneous elastic medium. The elastic constants and density of the spherical inclusion can be arbitrarily different from those of the surrounding medium. The sphere can also be filled with a fluid. The sphere is one of the few objects for which the scattering problem can be solved exactly. It also has the desirable property of being describable by a minimum number of parameters, which makes the interpretation of the analytical and numerical results relatively simple. Furthermore, scattering by a sphere represents a canonical problem for a more extended class of objects with relatively simple and smooth boundaries, and thus the results presented in this paper contribute to the general understanding of scattering from this class of heterogeneities.

2 THEORY

The analytical treatment of elastic wave scattering by a spherical inclusion has a long and rich history, dating back to the classical papers by Clebsch (1863) and Rayleigh (1871). Much of the earlier work was restricted to scalar (acoustic) waves, hollow inclusions, or rigid inclusions. There were also theoretical developments in the scattering of light waves, and a good summary of this work and the relevant references can be found in the book by Van der Hulst (1957). Considerable progress has been made in the use of asymptotic expansions which are appropriate at high frequencies, with the references in this area including Scholte (1956), Nussenzveig (1965, 1969), Ludwig (1970), Überall (1973), and Aki & Richards (1980). Much of the more recent work on the scattering of elastic waves by a spherical inclusion has been associated with the names of G. I. Petrashen in the USSR and R. Truell in the USA. As early as 1944 Petrashen was studying the scattering problem for an incident *P* wave, where he made use of a natural spherical vector system which he had developed earlier for the purposes of quantum mechanical problems. The later studies by Petrashen and his students were concerned mostly with obtaining asymptotic representations for different kinds of regular and diffracted waves formed by a sphere (Petrashen 1950; Buldyrev & Molotkov 1958), such as head interference waves for the scalar case (Buldyrev & Molotkov 1960), failure waves for the scalar case (Buldyrev 1964), surface waves on an isolated elastic sphere (Gelchinskij 1958), and complete solutions for an elastic sphere (Korneev 1983; Korneev & Petrashen 1987). Related work includes the theoretical and experimental studies of acoustic waves incident upon an elastic sphere by Nigul *et al.* (1974). Independently, Truell and his coworkers (Ying & Truell 1956; Einspruch, Witterholt & Truell 1960; Truell, Elbaum & Chick 1969) also made important contributions to the solution of this problem. Extensions and applications of this general approach can also be found in Yamakawa (1962). The basic equations that are obtained when displacement potentials are used along with summaries of some of the work mentioned above can be found in such books as Morse & Feshbach (1953) and Pao & Mow (1973).

The basic method followed in the above papers is to write the solutions inside and outside the inclusion in terms of appropriate eigenfunctions of the differential equations and then couple these solutions by matching the boundary conditions on the surface of the inclusion. It is also possible to formulate this problem as an integral equation by making use of the elastodynamic Green function for a homogeneous medium. Further information on this approach can be found in Miles (1960), Haddon & Cleary (1974), Varatharajulu & Pao (1976), Waterman (1976), Hudson (1977), Gubernatis, Domany & Krumhansl (1977a) and Gubernatis *et al.* (1977b).

In this section we outline a method of obtaining the general solution for the scattering of a plane *P* wave by a spherical inclusion. Although a solution to this problem can be found in several of the papers listed in the previous paragraphs, we repeat it here for completeness and also to introduce a set of spherical basis vectors which are used in our solution but are not common in the English literature. These basis vectors were developed by Petrashen and have properties which are convenient for solving vector function problems with spherical symmetry.

Consider the configuration shown in Fig. 1. Joint Cartesian $\{x, y, z\}$ and spherical $\{r, \theta, \phi\}$ coordinate systems will be used. Centred about the common origin of these coordinate systems is a sphere of radius $r = R$. The volume within this sphere will be denoted by the index $\nu = 1$, while the volume outside will be denoted by $\nu = 2$. The materials inside and outside the sphere will in general be different, and the properties of these materials are completely described by the Lame parameters and density

$$\lambda_\nu = \text{constant}, \qquad \mu_\nu = \text{constant}, \qquad \rho_\nu = \text{constant}, \qquad (\nu = 1, 2). \tag{2.1}$$

Incident from medium $\nu = 2$ is a harmonic disturbance with a displacement field given by

$$\tilde{\mathbf{U}}_0 = \mathbf{U}_0(x, y, z)e^{i\omega t}. \tag{2.2}$$

The interaction of this incident wave with the sphere gives rise to additional displacement fields both inside and outside the sphere, and these are denoted by

$$\tilde{\mathbf{U}}_\nu = \mathbf{U}_\nu(x, y, z)e^{i\omega t}, \qquad (\nu = 1, 2). \tag{2.3}$$

These additional disturbances will be referred to as the scattered fields. Associated with each field is a stress tensor. We will

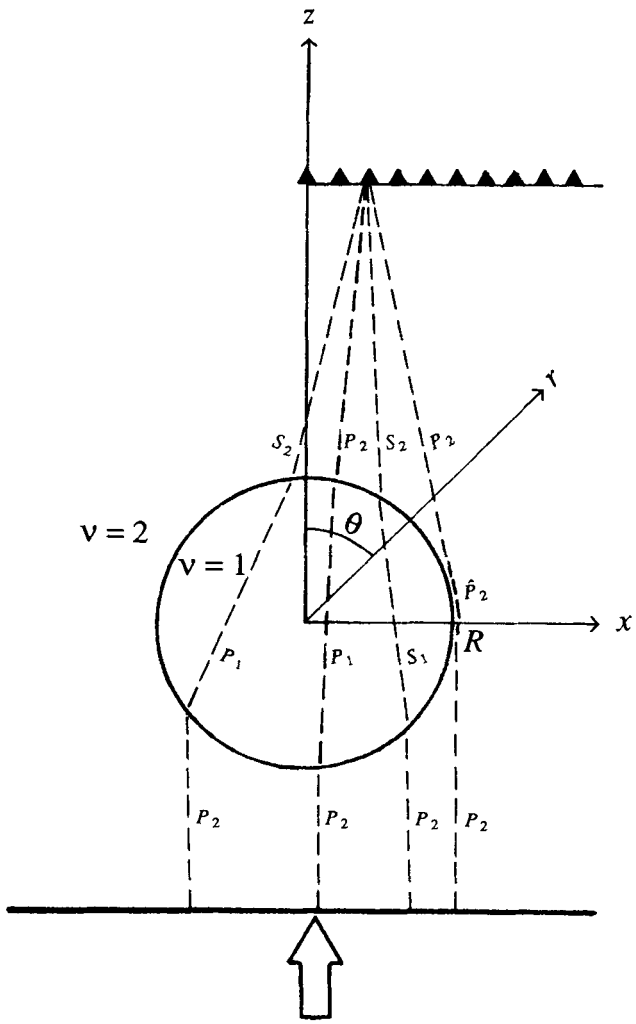

Figure 1. The geometry of the problem. The sphere of radius R has material properties denoted by $\nu = 1$, while the material properties of the surrounding medium are denoted by $\nu = 2$. A plane P wave is incident from along the negative z axis. The transmitted wave field is observed as a function of the x coordinate along a line that is offset a distance z from the centre of the sphere.

only need the traction on spherical surfaces and this is given by

$$t_r^{(\nu)}(\mathbf{U}_\nu) = \lambda_\nu \nabla \cdot \mathbf{U}_\nu \hat{\mathbf{r}} + 2\mu_\nu \frac{\partial \mathbf{U}_\nu}{\partial r} + \mu_\nu [\hat{\mathbf{r}} \times \nabla \times \mathbf{U}_\nu] \tag{2.4}$$

where $\hat{\mathbf{r}} = \mathbf{r}/r$ is the unit radius vector. We also denote the velocities and slowness of both compressional and shear waves by

$$V_p^{(\nu)} = \sqrt{\frac{\lambda_\nu + 2\mu_\nu}{\rho_\nu}} \equiv \alpha_\nu^{-1}, \qquad V_s^{(\nu)} = \sqrt{\frac{\mu_\nu}{\rho_\nu}} \equiv \beta_\nu^{-1}. \tag{2.5}$$

The incident field of eq. (2.2) and the scattered fields of eq. (2.3) must all satisfy the elastodynamic equations of motion in mediums $\nu = 1, 2$,

$$(\lambda_\nu + 2\mu_\nu)\nabla^2 \mathbf{U}_\nu - \mu_\nu \nabla \times \nabla \times \mathbf{U}_\nu + \rho_\nu \omega^2 \mathbf{U}_\nu = 0. \tag{2.6}$$

Taken together the fields must satisfy the boundary conditions on the surface of the sphere, which are that the displacement and traction should be continuous. Thus we require that

$$\mathbf{U}_1 = \mathbf{U}_0 + \mathbf{U}_2 \quad \text{and} \quad \mathbf{t}_r^{(1)}[\mathbf{U}_1] = \mathbf{t}_r^{(2)}[\mathbf{U}_0 + \mathbf{U}_2] \tag{2.7}$$

where all of these equations are evaluated at $r = R$. We also require that the scattered fields remain finite within the sphere and satisfy a radiation condition at large distances from the sphere

$$\mathbf{U}_2 \approx \frac{\mathbf{c}(\theta, \phi)}{r} e^{-ikr}, \qquad (r \to \infty) \tag{2.8}$$

where $k = \omega/V_p^{(2)}$ or $k = \omega/V_s^{(2)}$. This is a well-posed problem in that, given the incident wave, the boundary conditions are sufficient to solve for the scattered fields and thus arrive at a unique solution to the problem.

Now let us consider the special case of an incident wave which is a plane harmonic P (compressional) wave propagating in the direction of the positive z axis. In this case we have

$$\mathbf{U}_0 = \mathrm{e}^{-i\omega\alpha_2 z}\hat{\mathbf{z}} \tag{2.9}$$

where $\hat{\mathbf{z}}$ is a unit vector in the z direction. We construct the solutions by introducing the system of spherical vectors developed by Petrashen (1945, 1949)

$$\begin{aligned}
&\mathbf{Y}_{lm}^0 \equiv \mathbf{Y}_{lm}^0(\theta, \phi) = \mathbf{r} \times \nabla Y_{lm}(\theta, \phi) \\
&\mathbf{Y}_{lm}^+ \equiv \mathbf{Y}_{lm}^+(\theta, \phi) = (l+1)\hat{\mathbf{r}} Y_{lm}(\theta, \phi) - r\,\nabla Y_{lm}(\theta, \phi) \\
&\mathbf{Y}_{lm}^- \equiv \mathbf{Y}_{lm}^-(\theta, \phi) = l\hat{\mathbf{r}} Y_{lm}(\theta, \phi) + r\,\nabla Y_{lm}(\theta, \phi)
\end{aligned} \tag{2.10}$$

with the usual definitions for the spherical harmonic functions

$$Y_{lm}(\theta, \phi) = \mathrm{e}^{im\phi} P_l^m(\cos\theta), \qquad l \geq 0, \qquad (-l \leq m \leq l).$$

This system, whose main features are outlined in Appendix A, leads to particularly simple equations in this problem of spherical symmetry. Using the system of eq. (2.10), an arbitrary vector function $\mathbf{U}$ can be represented in the form

$$\mathbf{U} = \sum_{l \geq 0, |m| \leq l} \{\psi_{lm}^0(r)\mathbf{Y}_{lm}^0 + \psi_{lm}^+(r)\mathbf{Y}_{lm}^+ + \psi_{lm}^-(r)\mathbf{Y}_{lm}^-\} \tag{2.11}$$

where the $\psi_{lm}(r)$ are unspecified radial functions at this point.

The particular incident wave of eq. (2.9) has the representation

$$\mathbf{U}_0 = \sum_{l \geq 0} \{j_{l+1}(\omega\alpha_2 r)\mathbf{Y}_{l0}^+ - j_{l-1}(\omega\alpha_2 r)\mathbf{Y}_{l0}^-\} \exp\{-i[\pi/2(l+1)]\} \tag{2.12}$$

where the $j_k(x)$ are spherical Bessel functions. The displacement fields of the scattered waves $\mathbf{U}_1$ and $\mathbf{U}_2$ from eq. (2.3) can also be represented in terms of a series of the spherical vectors of eq. (2.10). Making use of the structure of the series in eq. (2.12) for the incident wave and the orthogonal properties of the spherical vectors (see Appendix A), it is possible to show that $\mathbf{U}_1$ and $\mathbf{U}_2$ can be expressed as

$$\begin{aligned}
\mathbf{U}_1 = \sum_{l \geq 0} &\{[a_l^{(1)} j_{l+1}(\omega\alpha_1 r) + l b_l^{(1)} j_{l+1}(\omega\beta_1 r)]\mathbf{Y}_{l0}^+ \\
&+ [-a_l^{(1)} j_{l-1}(\omega\alpha_1 r) + (l+1) b_l^{(1)} j_{l-1}(\omega\beta_1 r)]\mathbf{Y}_{l0}^-\} \exp\{-i[\pi/2(l+1)]\}
\end{aligned} \tag{2.13}$$

$$\begin{aligned}
\mathbf{U}_2 = \sum_{l \geq 0} &\{[a_l^{(2)} h_{l+1}(\omega\alpha_2 r) + l b_l^{(2)} h_{l+1}(\omega\beta_2 r)]\mathbf{Y}_{l0}^+ \\
&+ [-a_l^{(2)} h_{l-1}(\omega\alpha_2 r) + (l+1) b_l^{(2)} h_{l-1}(\omega\beta_2 r)]\mathbf{Y}_{l0}^-\} \exp\{-i[\pi/2(l+1)]\}
\end{aligned} \tag{2.14}$$

where $a_l^{(\nu)}$ and $b_l^{(\nu)}$ are now unknown scalars and the $h_k(x)$ are spherical Hankel functions of the second kind. Note that the spherical Bessel functions $j_k(x)$ of eq. (2.13) are finite throughout the inclusion and the spherical Hankel functions $h_k(x)$ of eq. (2.14) have asymptotic representations for a large argument that satisfy the condition in eq. (2.8). Also note that with the basis vectors being used here, the displacements in eqs (2.13) and (2.14) separate into compressional and shear fields, so that either equation can be put in the form

$$\mathbf{U}_\nu = \mathbf{U}_\nu^p + \mathbf{U}_\nu^s \tag{2.15}$$

with the $a_l^{(\nu)}$ associated with the P field $\mathbf{U}_\nu^p$ and the $b_l^{(\nu)}$ associated with the S field $\mathbf{U}_\nu^s$, and with the following conditions satisfied

$$\nabla \times \mathbf{U}_\nu^p \equiv 0, \qquad \nabla \cdot \mathbf{U}_\nu^s \equiv 0. \tag{2.16}$$

To determinate the coefficients $a_l^{(\nu)}$ and $b_l^{(\nu)}$ in eqs (2.13) and (2.14) we have to satisfy the boundary conditions of eq. (2.7). Making the necessary substitutions, evaluating the expressions for $r = R$, and using the orthogonal properties of the spherical vectors, one arrives at a separate set of linear equations for each value of l. When $l = 0$ one can take advantage of the fact that $\mathbf{Y}_{00}^- = 0$ to get the abbreviated set of equations

$$W_0 \begin{bmatrix} a_0^{(1)} \\ a_0^{(2)} \end{bmatrix} = \begin{bmatrix} j_1(\xi_2) \\ O_2 \end{bmatrix} \tag{2.17}$$

where

$$W_0 = \begin{bmatrix} j_1(\xi_1) - h_1(\xi_2) \\ \kappa O_1 - \tilde{O}_2 \end{bmatrix} \tag{2.18}$$

$$O_\nu = \frac{\gamma_\nu}{\xi_\nu}\left[\frac{\xi_\nu}{\gamma_\nu^2} j_0(\xi_\nu) - 4j_1(\xi_\nu)\right]$$

$$\tilde{O}_2 = \frac{\gamma_2}{\xi_2}\left[\frac{\xi_2}{\gamma_2^2} h_0(\xi_2) - 4h_1(\xi_2)\right]$$

$$\xi_\nu = \alpha_\nu \omega R, \qquad \eta_\nu = \beta_\nu \omega R \tag{2.19}$$

$$\gamma_\nu = \frac{\alpha_\nu}{\beta_\nu}, \qquad \kappa = \frac{\rho_1 \beta_2}{\rho_2 \beta_1}.$$

When $l \geq 1$ a full set of four equations with four unknowns is obtained of the form

$$W_l F_l = \tilde{F}_l \tag{2.20}$$

where F_l and $\tilde{F}_l$ are the column matrices

$$F_l = [a_l^{(1)}, b_l^{(1)}, a_l^{(2)}, b_l^{(2)}]^T \tag{2.21}$$

and

$$\tilde{F}_l = [j_{l+1}(\xi_2), -j_{l-1}(\xi_2), C_2^+, C_2^-]^T \tag{2.22}$$

and the matrix W_l is given by

$$W_l = \begin{bmatrix} j_{l+1}(\xi_1) & l j_{l+1}(\eta_1) & -h_{l+1}(\xi_2) & -l h_{l+1}(\eta_2) \\ -j_{l-1}(\xi_1) & (l+1) j_{l-1}(\eta_1) & h_{l-1}(\xi_2) & -(l+1) h_{l-1}(\eta_2) \\ \kappa C_1^+ & \kappa l D_1^+ & -\tilde{C}_2^+ & -l\tilde{D}_2^+ \\ \kappa C_1^- & -\kappa(l+1) D_1^- & -\tilde{C}_2^- & (l+1)\tilde{D}_2^- \end{bmatrix}. \tag{2.23}$$

The following notations are used here

$$\left.\begin{matrix} C_\nu^+ \\ C_\nu^- \end{matrix}\right\} = \frac{\gamma_\nu}{\xi_\nu}\left[\frac{\xi_\nu}{\gamma_\nu^2} j_l(\xi_\nu) - 2\left\{\begin{matrix} (l+2) j_{l+1}(\xi_\nu) \\ (l-1) j_{l-1}(\xi_\nu) \end{matrix}\right\}\right]$$

$$\left.\begin{matrix} \tilde{C}_\nu^+ \\ \tilde{C}_\nu^- \end{matrix}\right\} = \frac{\gamma_\nu}{\xi_\nu}\left[\frac{\xi_\nu}{\gamma_\nu^2} h_l(\xi_\nu) - 2\left\{\begin{matrix} (l+2) h_{l+1}(\xi_\nu) \\ (l-1) h_{l-1}(\xi_\nu) \end{matrix}\right\}\right]$$

$$\left.\begin{matrix} D_\nu^+ \\ D_\nu^- \end{matrix}\right\} = \frac{1}{\eta_\nu}\left[\eta_\nu j_l(\eta_\nu) - 2\left\{\begin{matrix} (l+2) j_{l+1}(\eta_\nu) \\ (l-1) j_{l-1}(\eta_\nu) \end{matrix}\right\}\right]$$

$$\left.\begin{matrix} \tilde{D}_\nu^+ \\ \tilde{D}_\nu^- \end{matrix}\right\} = \frac{1}{\eta_\nu}\left[\eta_\nu h_l(\eta_\nu) - 2\left\{\begin{matrix} (l+2) h_{l+1}(\eta_\nu) \\ (l-1) h_{l-1}(\eta_\nu) \end{matrix}\right\}\right].$$

It can be shown that the determinants of the matrices in eqs (2.18) and (2.23) are always different from zero, so in principle it is always possible to solve the systems of eqs (2.17) and (2.20) for the unknown coefficients $a_l^{(\nu)}$ and $b_l^{(\nu)}$ for any l. However, because of the asymptotic properties of the matrix elements, numerical difficulties can be encountered when solving these systems of equations. This will be discussed in the next section.

Finally, note that the coefficients $a_l^{(\nu)}$ and $b_l^{(\nu)}$ for any l are completely defined by the member of the series in eq. (2.12) for the incident wave with the same l. That is, there is no coupling between harmonics associated with different values of l. This means that a scattering problem for the sphere with an incident wave represented by any member of eq. (2.12) with index l could be considered, and the results would be the corresponding members of eqs (2.17) and (2.20) with the same index l. To illustrate this point we will show how the solution for an incident wave generated by a point pressure source can be obtained by a slight modification of the solution for the plane wave source developed above. Consider a point pressure source located at the point $\mathbf{R}_0 = (Z_0, 0, 0)$ where $Z_0 > R$. This will generate a displacement field $\mathbf{U}_0$ of a spherical P wave

$$\mathbf{U}_0 = -\nabla \frac{e^{-ik_p|\mathbf{r}-\mathbf{R}_0|}}{|\mathbf{r}-\mathbf{R}_0|} = -ik_p^2 \sum_{l\geq 0} \{j_{l+1}(k_p r)\mathbf{Y}_{l0}^+ - j_{l-1}(k_p r)\mathbf{Y}_{l0}^-\} h_l(k_p Z_0). \tag{2.24}$$

Each member of the series in eq. (2.24) differs from that in eq. (2.12) by the coefficient

$$c_l = -ik_p^2 e^{i[\pi/2(l+1)]} h_l(k_p Z_0).$$

Thus the solution for the point pressure source is simply obtained by multiplying the members of eqs (2.13) and (2.14) by c_l. The eqs (2.17) and (2.20) are unchanged.

3 NUMERICAL CONSIDERATIONS

To calculate the scattered fields $\mathbf{U}_1$ and $\mathbf{U}_2$ using the series in eqs (2.13) and (2.14) we have to solve the linear systems of eqs (2.17) and (2.20) for all $l \geq 0$. These systems of equations are generally solved by numerical methods, which means that the numerical stability of the calculations are a concern. The coefficients of the matrices W_l in these systems include spherical Bessel and Hankel functions, whose features for $l \gg 1$ are characterized by the formulae

$$j_l(z) \approx \frac{1}{z}\cos\left[z - [\pi/2(l+1)]\right], \qquad h_l(z) \approx \frac{1}{z}e^{-i\{z-[\pi/2(l+1)]\}} \tag{3.1}$$

if $z \gg l$, and

$$j_l(z) \approx \frac{1}{2z\sqrt{y}}\left(\frac{2y}{e}\right)^{-(l+1/2)}, \qquad h_l(z) \approx \frac{i}{z\sqrt{y}}\left(\frac{2y}{e}\right)^{l+1/2} \tag{3.2}$$

if $z \ll l$, where

$$y = \frac{l+\frac{1}{2}}{z}.$$

Because of different ratios between l and the arguments ξ_1, ξ_2, η_1 and η_2 of the functions j_l and h_l that appear in eq. (2.23), the orders of the different columns of this matrix can became quite different. In particular, for the case $l \to \infty$ the coefficients in the two first columns go to zero while the other coefficients go to infinity. In such a situation numerical calculations on a computer can become unstable before achieving the necessary accuracy.

To avoid this situation, we redefine the unknown variables $a_l^{(\nu)}$, $b_l^{(\nu)}$ as new ones $x_l^{(\nu)}$, $y_l^{(\nu)}$with the formulae

$$\begin{aligned} a_l^{(1)} &= h_l(\xi_1)x_1^{(1)}, \qquad b_l^{(1)} = h_l(\eta_1)y_1^{(1)} \\ a_l^{(2)} &= h_l^{-1}(\xi_2)x_1^{(2)}, \qquad b_l^{(2)} = h_l^{-1}(\eta_2)y_1^{(2)}. \end{aligned} \tag{3.3}$$

Now, if we let the unknown column matrix be

$$X_l = [x_l^{(1)}, y_l^{(1)}, x_l^{(2)}, y_l^{(2)}]^T \tag{3.4}$$

the system of eq. (2.20) will be

$$\tilde{W}_l X_l = \tilde{F}_l \tag{3.5}$$

where the column matrix $\tilde{F}_l$ is the same as in eq. (2.22), and $\tilde{W}_l$ can be obtained from eq. (2.23) by multiplying its columns by $h_l(\xi_1)$, $h_l(\eta_1)$, $h_l^{-1}(\xi_2)$, $h_l^{-1}(\eta_2)$, respectively. Now the coefficients of the matrix $\tilde{W}_l$ have values of approximately the same order (they differ from each other no more than by a coefficient of order l) and the numerical difficulty mentioned above is avoided.

The change in variable given by eq. (3.3) is also helpful in solving another numerical problem, that of determining how much of the infinite series in eqs (2.13) and (2.14) must be retained in order to achieve a given accuracy. Note that the unknown coefficients now are of the same order as the members of $\tilde{F}_l$

$$x_l^{(\nu)} \sim y_l^{(\nu)} \sim j_l(\xi_2) \tag{3.6a}$$

and for $l > \xi_2$ we obtain the estimate

$$x_{l_0}^{(\nu)} \sim y_{l_0}^{(\nu)} \sim \frac{1}{2\sqrt{\xi_2 l_0}}\left[1 - \frac{N+\frac{1}{2}}{l_0+\frac{1}{2}}\right]^{l_0+1/2} \approx \frac{1}{2\sqrt{\xi_2 l_0}}e^{-N} \tag{3.6b}$$

where

$$l_0 = \frac{e\xi_2}{2} + N, \qquad (N > 1) \tag{3.7}$$

is taken to be sufficiently large ($l_0 \gg 1$). Thus, the coefficients $x_l^{(\nu)}$ and $y_l^{(\nu)}$ go to zero exponentially when $l \geq e\xi_2/2 + N$ and $N \to \infty$. Using the following relations obtained from eq. (3.3)

$$\left.\begin{aligned} a_l^{(1)} j_{l\pm1}(\omega\alpha_1 r) &= x_l^{(1)} h_l(\xi_1) j_{l\pm1}\left(\xi_1 \frac{r}{R}\right) \\ b_l^{(1)} j_{l\pm1}(\omega\beta_1 r) &= y_l^{(1)} h_l(\eta_1) j_{l\pm1}\left(\eta_1 \frac{r}{R}\right) \end{aligned}\right\} \quad (r < R)$$

$$\left.\begin{aligned} a_l^{(2)} h_{l\pm1}(\omega\alpha_2 r) &= x_l^{(2)} h_{l\pm1}\left(\xi_2 \frac{r}{R}\right) \Big/ h_l(\xi_2) \\ b_l^{(2)} h_{l\pm1}(\omega\beta_2 r) &= y_l^{(2)} h_{l\pm1}\left(\eta_1 \frac{r}{R}\right) \Big/ h_l(\eta_2) \end{aligned}\right\} \quad (r > R)$$

and the 'limited' character of the values

$$\left|h_{l\pm1}\left(\xi\frac{r}{R}\right)\Big/h_l(\xi)\right|, \qquad \left|h_l(\xi)j_{l\pm1}\left(\xi\frac{r}{R}\right)\right|$$

it is clear that the series in eqs (2.13) and (2.14) converge at a rate that is equal to or greater than the series in eq. (2.12). Therefore, if we take the first l_0 members of the series, with l_0 specified by eq. (3.7), the absolute error of the calculations will not be greater than a value of order e^{-N}. When any of the arguments ξ_ν, η_ν is no more than ξ_2, the error in the respective series decreases with increasing r as $(r/R)^{l_0}$ in medium $\nu = 1$ $(r < R)$ and as $(R/r)^{l_0}$ in medium $\nu = 2$ $(r > R)$. Thus, given an error tolerance for the calculations of the fields $\mathbf{U}_\nu(r, \theta)$, we can estimate a number l_0 for any frequency ω and sum the series in eqs (2.13) and (2.14) for $l \leq l_0$. Test calculations showed that $N = 15$ in eq. (3.7) is sufficient to give an accuracy of 10^{-8} or better.

As mentioned at the beginning of this section, the system of eqs (2.20), or equivalently (3.5), are generally solved by numerical methods. However, analytical solutions of these systems are possible, although laborious, requiring the equivalent of inverting a matrix of rank four. This has been done and the results are given in Appendix B. Having two different solutions of the same basic equations is quite useful in checking the stability and accuracy of both solutions. Thus the analytical solutions of Appendix B were used to check the solutions that were obtained by numerically solving eq. (3.5). This comparison showed that for l_0 given by eq. (3.7) with $N = 15$ the numerical solution of eq. (3.5) is stable and gives the same result as the analytical solutions. For $N > 15$ (accuracies better than 10^{-8}) the calculations revealed that the analytical solution gave more accurate results. It should be mentioned here that all of the calculations discussed in this paper were done with double precision arithmetic.

There is another way of estimating the accuracy of the calculations without considering the properties of the coefficients a_l and b_l. This approach takes advantage of the observation made earlier that there is no coupling between harmonics associated with different values of l. Thus one considers the expression for the incident wave in eq. (2.12) evaluated on the surface of the sphere $(r = R)$ and truncates the series at a value of l that gives the desired accuracy in representing the incident wave. Then the a_l and b_l summed up to this same value of l can be considered as either the exact solution to the truncated version of the incident wave or as the approximate solution to the analytical version of the incident wave having the desired accuracy.

4 SCATTERING CROSS-SECTIONS

A useful method of characterizing scattering by an object is to calculate the energy of the scattered waves and compare it to the energy of the incident wave. Various forms of this ratio between the scattered and incident energies are called scattering cross-sections. The energy of the scattered waves can be obtained by calculating the energy flux of scattered waves through a surface S that completely surrounds the object. Noting that the energy flux per unit time through a surface element ds having a normal $\mathbf{n}$ is given by $(\dot{\mathbf{U}} \cdot t_n[\mathbf{U}])$ and that the energy flux averaged over one period is $\omega\, \mathcal{I}m\, (\mathbf{U} \cdot t_n^*[\mathbf{U}])/2$, then the total energy flux per period through the surface S is given by

$$F = \frac{\omega}{2}\, \mathcal{I}m \int_S (\mathbf{U} \cdot t_n^*[\mathbf{U}])\, ds \tag{4.1}$$

where (*) means the complex conjugate. The same reasoning applied to the incident P wave yields an energy flux per unit area of the wavefront of $\omega^2\alpha_2(\lambda_2 + 2\mu_2)/2$.

Now we follow Truell *et al.* (1969) and define a normalized cross-section as the ratio of the flow of total energy carried outward by the scattered waves to the rate of flow in the incident wave through a normal area equal to the cross-sectional area of the object (geometric shadow of the object). In our case we let S be a spherical surface of radius r_0 with $r_0 > R$ and the normalized cross-section is given by

$$\sigma_N = \mathcal{I}m \int_{r=r_0} \frac{\Phi\, ds}{\omega\alpha_2(\lambda_2 + 2\mu_2)\pi R^2}$$

where Φ can be calculated by using either of the formulae

$$\Phi = (\mathbf{U}_2 \cdot \mathbf{t}_r^*[\mathbf{U}_2]) \tag{4.2a}$$

or

$$\Phi = -(\mathbf{U}_2 \cdot \mathbf{t}_r^*[\mathbf{U}_0]) - (\mathbf{U}_0 \cdot \mathbf{t}_r^*[\mathbf{U}_2]). \tag{4.2b}$$

The second expression for Φ is easily obtained from the fact that the scatterer generates no additional energy, which leads to the conditions which for both the incident wave $\mathbf{U}_0$ and the total field $\mathbf{U}_0 + \mathbf{U}_2$ there is zero net energy flux across the surface S so long as it is entirely contained in medium $\nu = 2$.

Using eq. (2.4) for the traction vector, the series in eqs (2.12) and (2.14) for $\mathbf{U}_0$ and $\mathbf{U}_2$ and orthogonal properties of the

spherical vectors, we can obtain two different expressions for σ_N

$$\sigma_N = 4\sum_{l\geq 0}^{\infty}(2l+1)\left\{\left|\frac{a_l^{(2)}}{\xi_2}\right|^2 + l(l+1)\gamma_2\left|\frac{b_l^{(2)}}{\eta_2}\right|^2\right\} \tag{4.3a}$$

or

$$\sigma_N = -4\sum_{l\geq 0}^{\infty}(2l+1)\frac{\mathscr{R}e\, a_l^{(2)}}{\xi_2^2}. \tag{4.3b}$$

This result together with the earlier noted fact that the coefficients for different values of l are not coupled means that we must have

$$|a_l^{(2)}|^2 + l(l+1)\gamma_2^3|b_l^{(2)}|^2 = -\mathscr{R}e\, a_l^{(2)} \tag{4.4}$$

for any value of l. This relationship is useful in verifying numerical calculations.

The function σ_N from eq. (4.3) is closely connected with the value of the field $\mathbf{U}_2(r, \theta)$ of scattered waves that is observed along the positive z axis for large r ($r \gg 2\pi V_p/\omega$). Using asymptotic expressions for the spherical Hankel functions in eq. (2.14) we obtain

$$\begin{aligned}\mathbf{U}_2(r, 0) &= i\hat{\mathbf{z}}\frac{e^{i\xi_2(r/R)}}{\xi_2 r}R\sum_{l\geq 0}(2l+1)a_l^{(2)}\left[1+O\left(\frac{1}{r}\right)\right]\\ &= \hat{\mathbf{z}}\frac{e^{-i\xi_2(r/R)}}{r}A_0\left[1+O\left(\frac{1}{r}\right)\right]\end{aligned} \tag{4.5}$$

where

$$A_0 = i\frac{R}{\xi_2}\sum_{l\geq 0}(2l+1)a_l^{(2)}.$$

Comparing eq. (4.5) with (4.3b) we have

$$\sigma_N = -4\frac{\mathscr{I}m\{A_0\}}{R\xi_2} \tag{4.6}$$

which is analogous to an optical theorem for elastodynamics. This expression in eq. (4.6) is a useful relationship between the amplitude of the forward-scattered field and the total energy scattered in all directions by the obstacle.

5 NUMERICAL RESULTS

One of the primary purposes of this investigation was to gain an understanding of the features of waves scattered by a local spherical heterogeneity. This problem can be studied with approximate methods, such as ray theory, but it is not always clear if the information provided about amplitudes and waveforms is accurate. With the results presented earlier in this paper, it is possible to calculate these scattered waves with the assurance that the results are complete and accurate. Unfortunately, the results such as eqs (2.13) and (2.14) are not very revealing in the form of an analytical series and must first be converted to some graphical form, such as synthetic seismograms or scattering cross-sections, before the physical properties of the scattered waves become apparent.

We are interested in knowing what types of waves are scattered by a sphere and particularly interested in understanding where the scattered waves with the largest amplitudes can be found in the region surrounding the sphere. It is possible to argue that the main features of such waves that are scattered by a sphere will be approximately the same for a wide class of smoothly shaped 3-D heterogeneities, and this broadens the utility of the results presented in this paper for providing insight into realistic seismological problems.

First consider the matter of what types of waves are scattered by the sphere and their relative amplitudes. These effects are best observed in the time domain, which requires that the frequency domain solutions obtained in this paper be transformed to the time domain. This was done by applying a numerical Fourier transform to the solutions and by assuming a broad-band pulse as the form of the input wave. This source pulse had constant amplitudes in the frequency band between 0.00 and 64.0 Hz with a sampling interval of 0.25 Hz, which means that the pulse contained wavelengths that ranged from more than one order of magnitude smaller than the radius of the sphere to more than an order of magnitude larger. Synthetic seismograms were calculated for the positions that are shown in Fig. 1, which lie on a line offset a distance z from the centre of the sphere in the direction of forward scattering and extending from the centre of the shadow into the fully illuminated zone. Because of the symmetry of the problem, there are only two non-zero components to the solutions, $U_x = U_x(x, 0, z, t)$ and $U_z = U_z(x, 0, z, t)$.

The solutions presented in this paper can be calculated for arbitrary elastic properties inside and outside the sphere,

including the case of a fluid inside the sphere. Here we present results for two models, one representing a low-velocity scatterer and the other representing a high-velocity scatterer. The elastic parameters for these two models are as follows:

model 1 $V_p^{(1)} = 4.5\ \mathrm{km\ s^{-1}}$, $V_s^{(1)} = 2.6\ \mathrm{km\ s^{-1}}$, $\rho_1 = 2.3\ \mathrm{gm\ cm^{-3}}$

$V_p^{(2)} = 6.0\ \mathrm{km\ s^{-1}}$, $V_s^{(2)} = 3.5\ \mathrm{km\ s^{-1}}$, $\rho_2 = 2.7\ \mathrm{gm\ cm^{-3}}$

model 2 $V_p^{(1)} = 7.5\ \mathrm{km\ s^{-1}}$, $V_s^{(1)} = 4.4\ \mathrm{km\ s^{-1}}$, $\rho_1 = 3.1\ \mathrm{gm\ cm^{-3}}$

$V_p^{(2)} = 6.0\ \mathrm{km\ s^{-1}}$, $V_s^{(2)} = 3.5\ \mathrm{km\ s^{-1}}$, $\rho_2 = 2.7\ \mathrm{gm\ cm^{-3}}$

Note that there is only one physical dimension in this problem, the radius of the sphere R. Thus all of the other parameters in the problem can be scaled with respect to this parameter, which is given a value of unity in the results that follow. The velocities and frequencies scale with R in the sense that the results are invariant so long as the expressions of eq. (2.19) and the ratio r/R remain constant.

Synthetic seismograms are shown for three different values of the offset distance from the sphere z in Figs 2, 3, and 4. The results for the low-velocity scatterer (model 1) are shown in the upper parts of these figures and those for a high-velocity scatterer (model 2) are shown in the lower parts. In all of these figures a distance of 1 km along the x axis represents the edge of the geometrical shadow, since the value $R = 1$ km was used for the radius of the sphere.

It is useful to associate geometrical ray paths with the primary features of the synthetic seismograms. Within the forward shadow there are three main types of scattered waves. These are (see Fig. 1): (1) a compressional refracted wave $P_2P_1P_2$ that goes through the sphere. (2) A shear refracted wave that goes through the sphere as $P_2P_1S_2$ for a low-velocity sphere and as

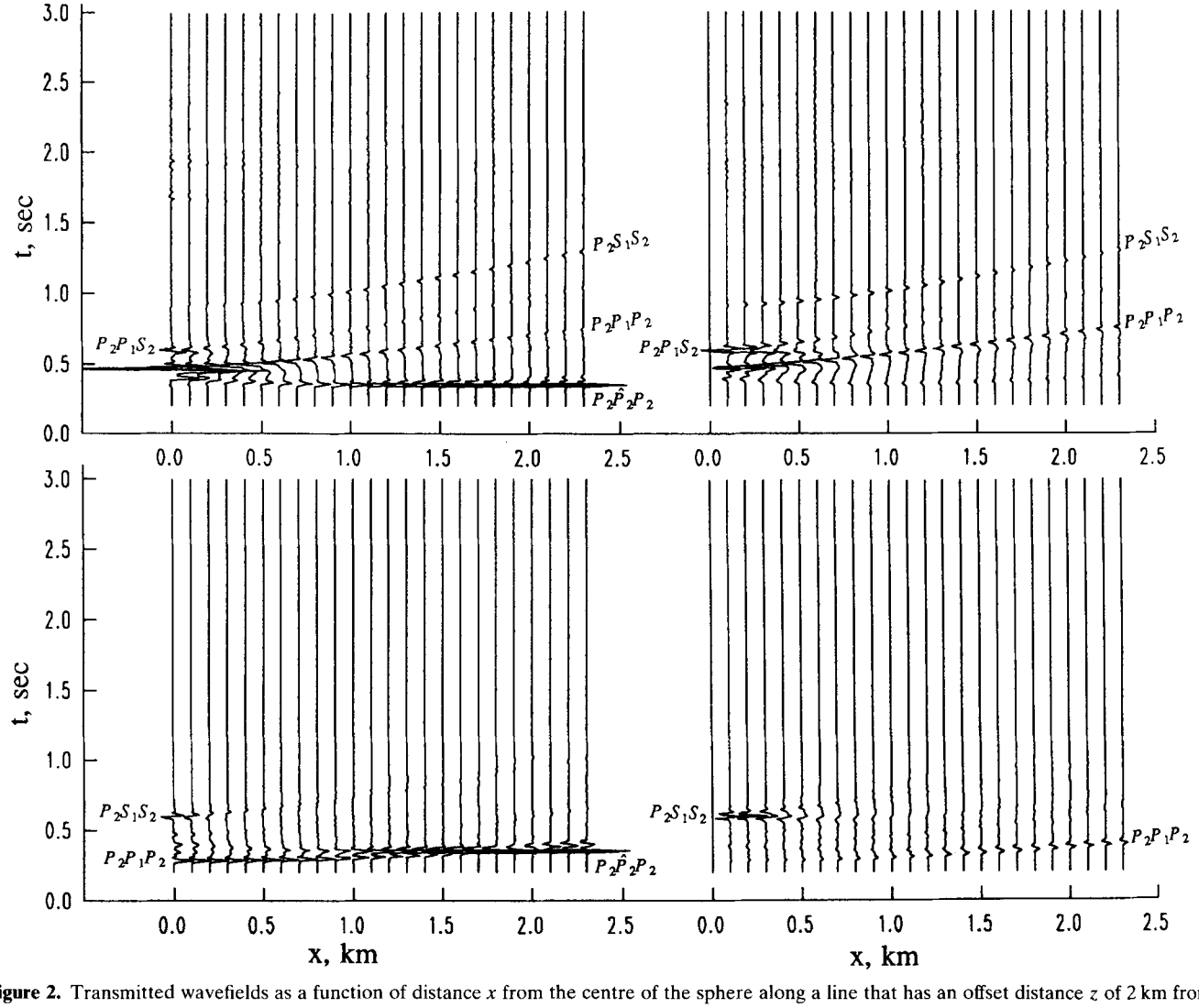

Figure 2. Transmitted wavefields as a function of distance x from the centre of the sphere along a line that has an offset distance z of 2 km from the centre of a sphere having a radius $R = 1$ km (see Fig. 1 for geometry). The panels on the left are for the z components of motion and the panels on the right are for the x components of motion. The top two panels are for model 1 of a low-velocity inclusion, and the bottom two panels are for model 2 of a high-velocity inclusion. The distance $x = 1$ corresponds to the edge of the geometrical shadow.

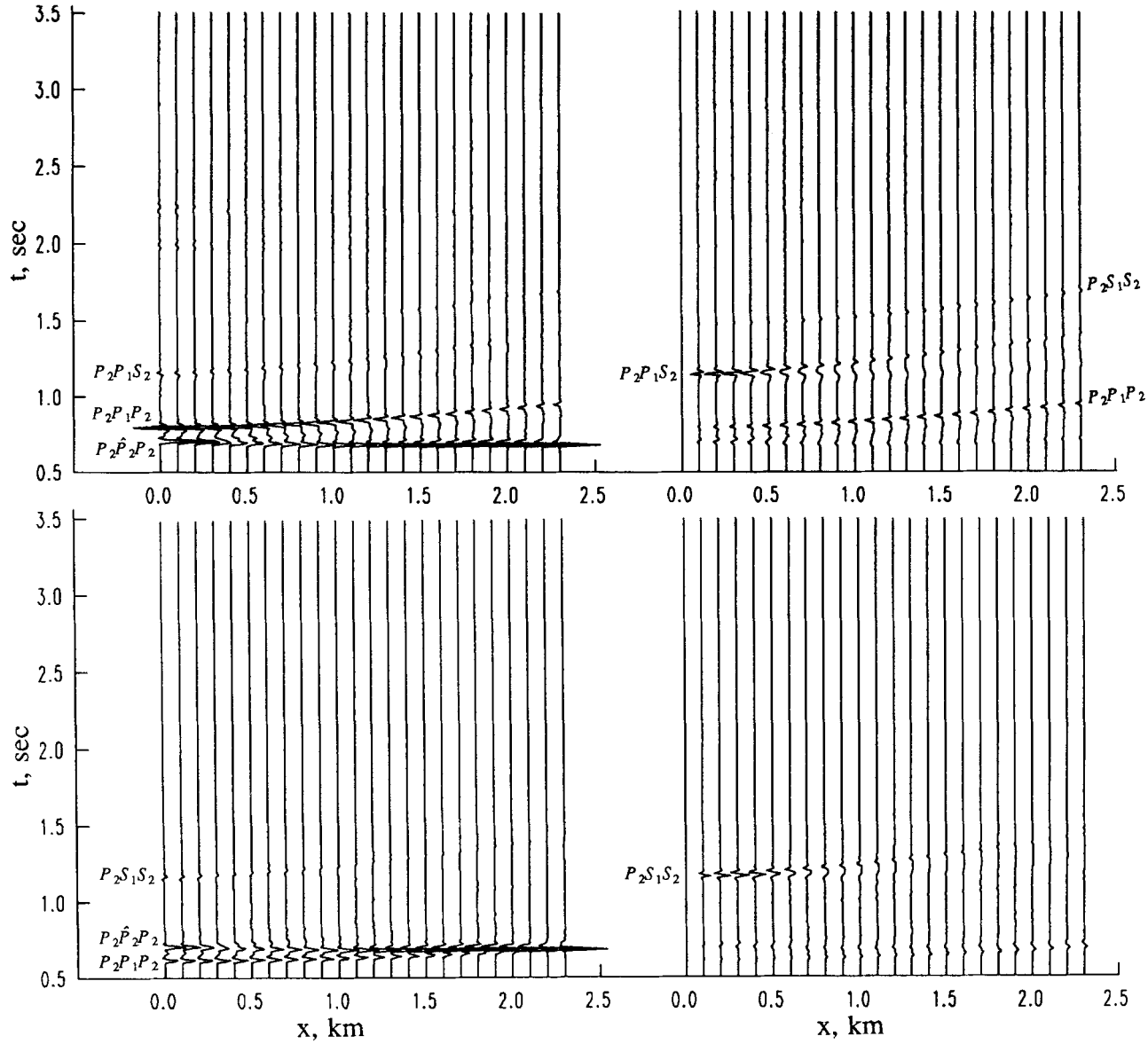

Figure 3. Similar to Fig. 2 except that the offset distance z is 4 km.

$P_2S_1S_2$ for a high-velocity sphere. (3) A compressional diffracted wave $P_2\hat{P}_2P_2$ that goes around the surface of the sphere. The relative contributions of these different waves to the total seismogram depends upon the offset distance z from the centre of the sphere.

For near-offset distances $z = 2R$ (Fig. 2), the wave $P_2P_1P_2$ dominates the first arrivals within the shadow on the z component. For a low-velocity sphere (model 1) it has a reversed polarity and arrives after the wave diffracted around the outside of the sphere. Note that there is a strong focusing along the axis for the low-velocity sphere but not the high-velocity sphere. The diffracted wave $P_2\hat{P}_2P_2$ has a smaller amplitude within the deep shadow at this offset distance. This low-frequency wave loses amplitude exponentially along its ray path around the sphere and is delayed in time with respect to the undisturbed incident wave. The shear waves $P_2P_1S_2$ (low-velocity case) and $P_2S_1S_2$ (high-velocity case) are strong on the x component and have a compound wave structure, involving a caustic and two diffracted waves. The caustic is due to the fact that the sphere is a low-velocity zone for both of these waves, and extending beyond this caustic are low-frequency diffracted waves that attenuate rapidly with distance. For the low-velocity sphere this diffraction from the caustic begins to interfere with the $P_2P_1P_2$ wave at this offset distance. Behind this caustic and its diffraction is the wave that has been refracted through the opposite side of the sphere and thus arrives at a later time. Along this branch of the wave there is a transition from a geometrical ray arrival to a diffracted wave that continues on to greater distances, although the point of this transition is not obvious on the seismograms. Note that, because of focusing effects and near-field terms that are important at this offset distance, these waves have significant amplitudes on the z component of motion near the centre of the shadow. In fact, at $x = 0$, we have the unusual situation of an S wave that appears only on the z component.

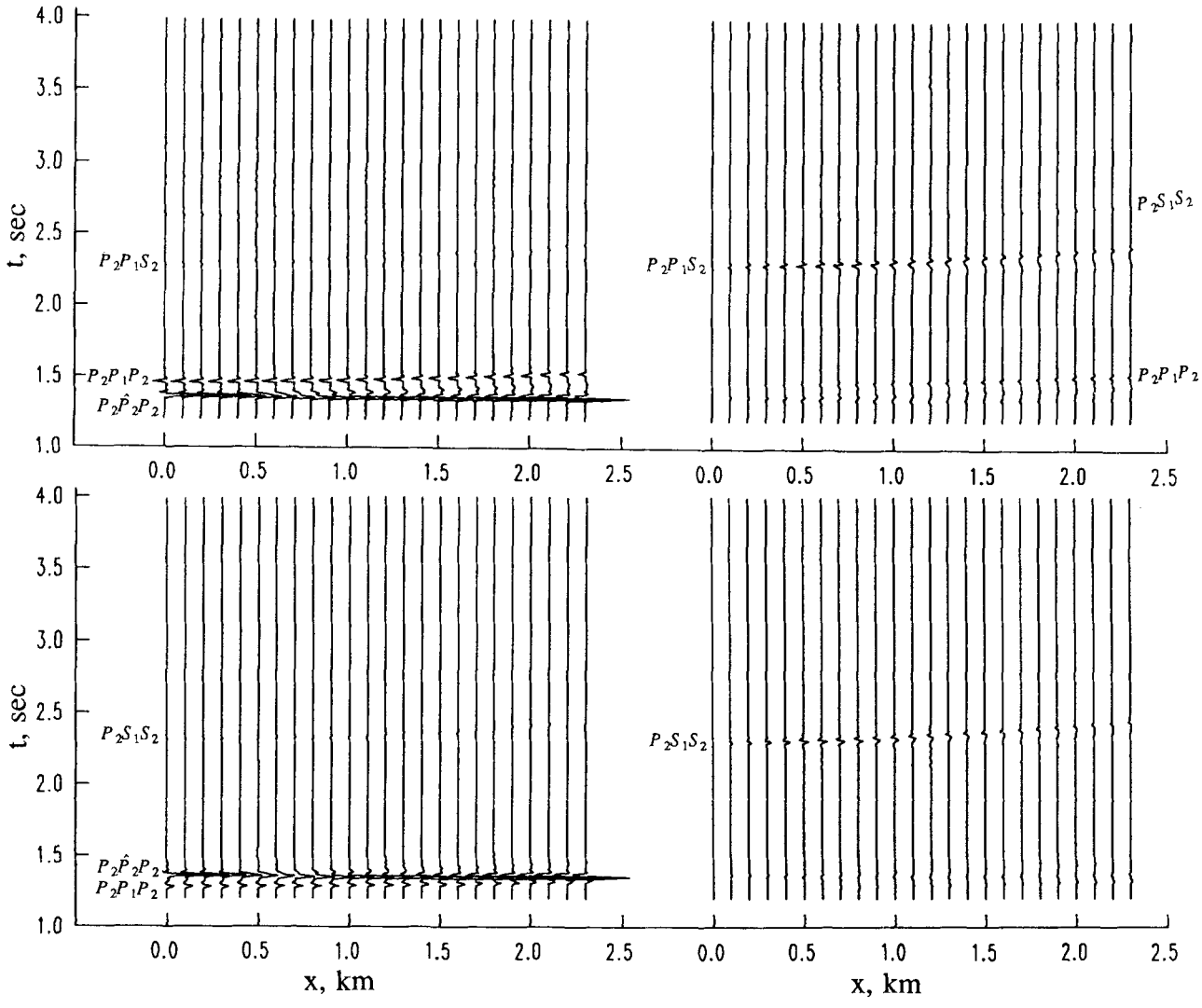

Figure 4. Similar to Fig. 2 except that the offset distance z is 8 km.

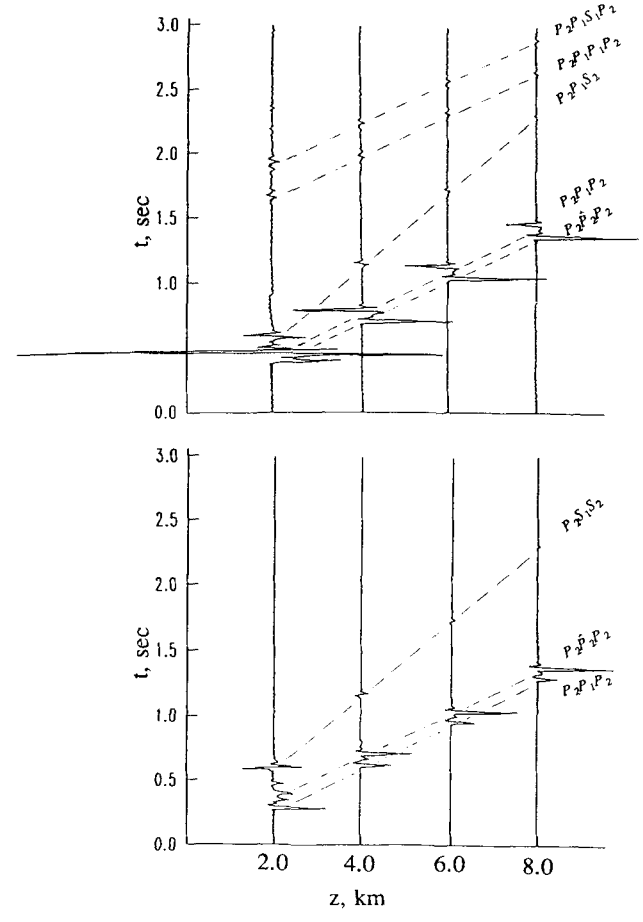

Figure 5. Transmitted wavefields in the deepest shadow of the sphere ($x = 0$) as a function of the offset distance z. Only the z component of the field is shown, as the x component is identically zero. The upper panel is for model 1 of a low-velocity inclusion, and the lower panel is for model 2 of a high-velocity inclusion.

For medium offset distances $z = 4R$ (Fig. 3), all three of the waves $P_2P_1P_2$, $P_2\hat{P}_2P_2$, and $P_2S_1S_2$ have comparable amplitudes. The waves $P_2P_1P_2$ and $P_2\hat{P}_2P_2$ arrive closely in time and interfere with each other. The $P_2P_1S_2$ and $P_2S_1S_2$ waves are now separated in time from the other phases and their compound nature is clearly evident.

For the larger offset distances $z = 8R$ (Fig. 4), the wave $P_2\hat{P}_2P_2$ is dominant on the z components, as the shadow is not nearly so deep as at the smaller offset distances. The wave $P_2P_1P_2$ which has passed through the sphere is relatively small compared to the wave which has diffracted around it. On the x components the waves $P_2P_1S_2$ and $P_2S_1S_2$ are the dominant arrivals and still display their compound waveforms. It is worth commenting on the reason why the $P_2P_1S_2$ wave is the dominant shear wave arrival for the low-velocity case, while $P_2S_1S_2$ is dominant for the high-velocity case. These are the S waves that see the smallest change in material properties upon both entering and leaving the sphere, and thus the amount of energy lost to reflection and also the amount of strong focusing is minimized. In contrast, the wave $P_2S_1S_2$ for the low-velocity case encounters a large change in velocity upon entering the sphere, which leads to more energy lost to reflected waves and also causes focusing so strong that the focal point lies within the sphere. Likewise, the wave $P_2P_1S_2$ for the high-velocity case encounters a large change in velocity upon leaving the sphere.

It should be emphasized that, regardless of the distance from the scatterer, there is a significant amount of motion on the x component. Recall that the displacement on this component would be zero if the sphere were not present, so we see that scattering is an effective means of transferring motion from one component of motion to an orthogonal component in the direction of forward propagation. At the larger offset distances and for both the low-velocity case and the high-velocity case, the shear waves are the dominant contributor to the x-component seismograms.

A slightly different presentation of some of the data from Figs 2, 3 and 4 is shown in Fig. 5. Here the seismograms for the z component at the centre of the shadow are shown as a function of the offset distance z. They show quite clearly how the dominant wave type in the shadow changes from $P_2P_1P_2$ at small z to $P_2\hat{P}_2P_2$ at large z for the cases of both the low-velocity inclusion and the high-velocity inclusion. Note that for the low-velocity inclusion the $P_2\hat{P}_2P_2$ wave is the first arrival, whereas for the high-velocity sphere it is the $P_2P_1P_2$ wave that arrives first. This figure also illustrates how the low-velocity sphere is much effective in focusing energy into the shadow than is the high-velocity sphere.

These results show that, depending upon the distance of the observation point from the scattering object, the dominant part of the seismic field in the shadow zone may be composed of waves having a fundamentally different nature. Moreover, in the case of low frequencies it may be difficult to separate these different waves from each other on the basis of traveltimes. It would appear that results of this type would be applicable to various types of seismic tomographic methods. For instance, the results in Fig. 5 show quite clearly that at observation points distant from the inclusion more than a few times its dimension, the dominant wave has been diffracted around the obstacle rather than passing through it, which differs from the common assumption made in seismic transmission tomography. Because of this, the traveltime anomaly will decrease with distance from the inclusion. Obviously, when solving inverse problems to obtain estimates of the properties of the scattering object, it is important to have a proper understanding of what types of waves are dominating the seismograms in order that the correct algorithms can be applied.

So far we have considered only forward scattered waves and the results have been illustrated with broad-band time domain seismograms. To obtain a better understanding of how the scattered fields depend upon frequency and also to expand the spatial coverage to include back-scattered waves, it is convenient to consider scattering diagrams. The field $\mathbf{U}_2$ from eq. (2.14) can be represented in the form

$$\mathbf{U}_2 = [\mathbf{U}_p(\theta)]_r\hat{\mathbf{r}} + [\mathbf{U}_p(\theta)]_\theta\hat{\boldsymbol{\theta}} + [\mathbf{U}_s(\theta)]_r\hat{\mathbf{r}} + [\mathbf{U}_s(\theta)]_\theta\hat{\theta}. \tag{5.1}$$

Then, using eq. (2.14) and the definitions of the spherical vectors, we obtain the following expressions for the scattering diagrams for the P and S fields

$$[\mathbf{U}_p(\theta)]_r = -\sum_{l\geq 0} a_l^{(2)}(2l+1)e^{-i[\pi/2(l+1)]}\frac{\partial h_l(\xi)}{\partial \xi}P_l(\cos\theta)$$

$$[\mathbf{U}_p(\theta)]_\theta = -\sum_{l\geq 0} a_l^{(2)}(2l+1)e^{-i[\pi/2(l+1)]}\frac{h_l(\xi)}{\xi}\frac{\partial P_l(\cos\theta)}{\partial\theta}$$

$$[\mathbf{U}_s(\theta)]_r = \sum_{l\geq 1} b_l^{(2)}l(l+1)(2l+1)e^{-i[\pi/2(l+1)]}\frac{h_l(\eta)}{\eta}P_l(\cos\theta) \tag{5.2}$$

$$[\mathbf{U}_s(\theta)]_\theta = \sum_{l\geq 1} b_l^{(2)}(2l+1)e^{-i[\pi/2(l+1)]}\left(\frac{\partial h_l(\eta)}{\partial\eta} + \frac{h_l(\eta)}{\eta}\right)\frac{\partial P_l(\cos\theta)}{\partial\theta}$$

where we have assumed that the parameters

$$\xi = \frac{\omega r}{V_p^{(2)}}, \qquad \eta = \frac{\omega r}{V_s^{(2)}} \tag{5.3}$$

are evaluated for any $r > R$.

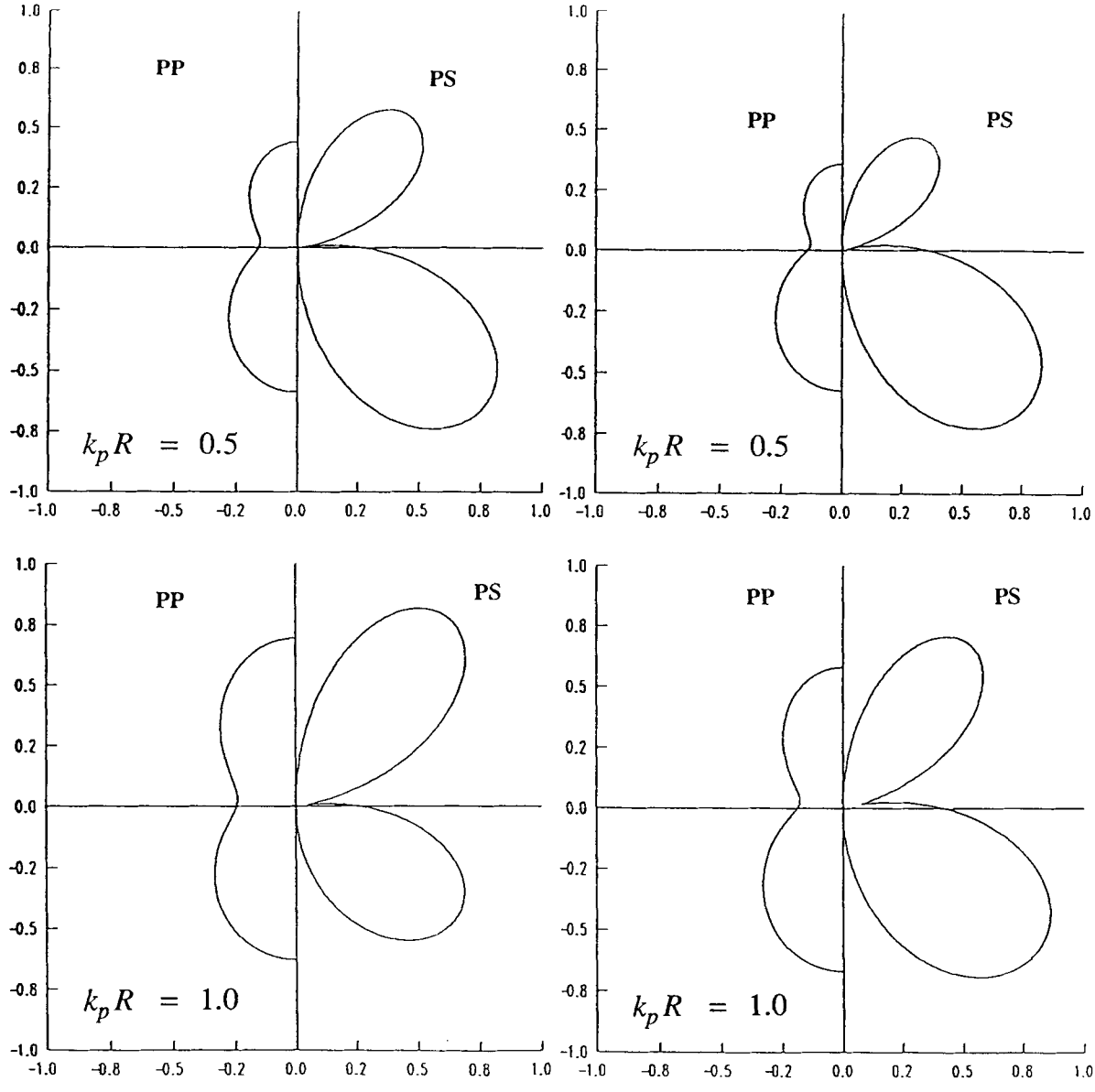

Figure 6(a). Scattering diagrams for various values of the parameter $k_pR = \omega R/V_p$. In each panel the left-hand figure represents the scattered P field, while the right-hand figure represents the scattered S field. The top two panels are for the case $k_pR = 0.5$ and the bottom two panels are for the case $k_pR = 1.0$. The two panels on the left are for model 1 of a low-velocity inclusion, and the two panels on the right are for model 2 of a high-velocity inclusion.

Scattering diagrams for six different ratios of R/λ that range from less than 0.1 to greater than 3.0 and for both models are shown in Fig. 6, where the radius of the observation point r is taken large enough that near-field terms are small and the scattered P and S waves have their natural polarizations. A number of interesting results emerge from the study of these figures. First, at low frequencies more of the incident P field is converted to scattered S fields than to scattered P fields, while at high frequencies just the opposite occurs. Second, at low frequencies the portions of the incident field which are forward scattered and back scattered are comparable, whereas at high frequencies most of the scattered field lies in the forward direction. At the highest frequencies we approach the case of only generating a forward-scattered P field. Third, in terms of the shapes and amplitudes of the scattering diagrams, there are only minor differences between the case of the low-velocity inclusion and that of the high-velocity inclusion. This is consistent with the results shown in Figs 2–5, where the differences between the low- and high-velocity case are most pronounced at small distances from the inclusion and tend to diminish at larger distances. Obviously, the near-field parts of the solution are more sensitive to the sign of the velocity anomaly of the inclusion than are the far field parts.

Finally, to obtain even more detailed information about the frequency dependence of the scattered fields, it is instructive to consider the scattering cross-sections defined in Section 4. These scattering cross-sections are plotted for both the

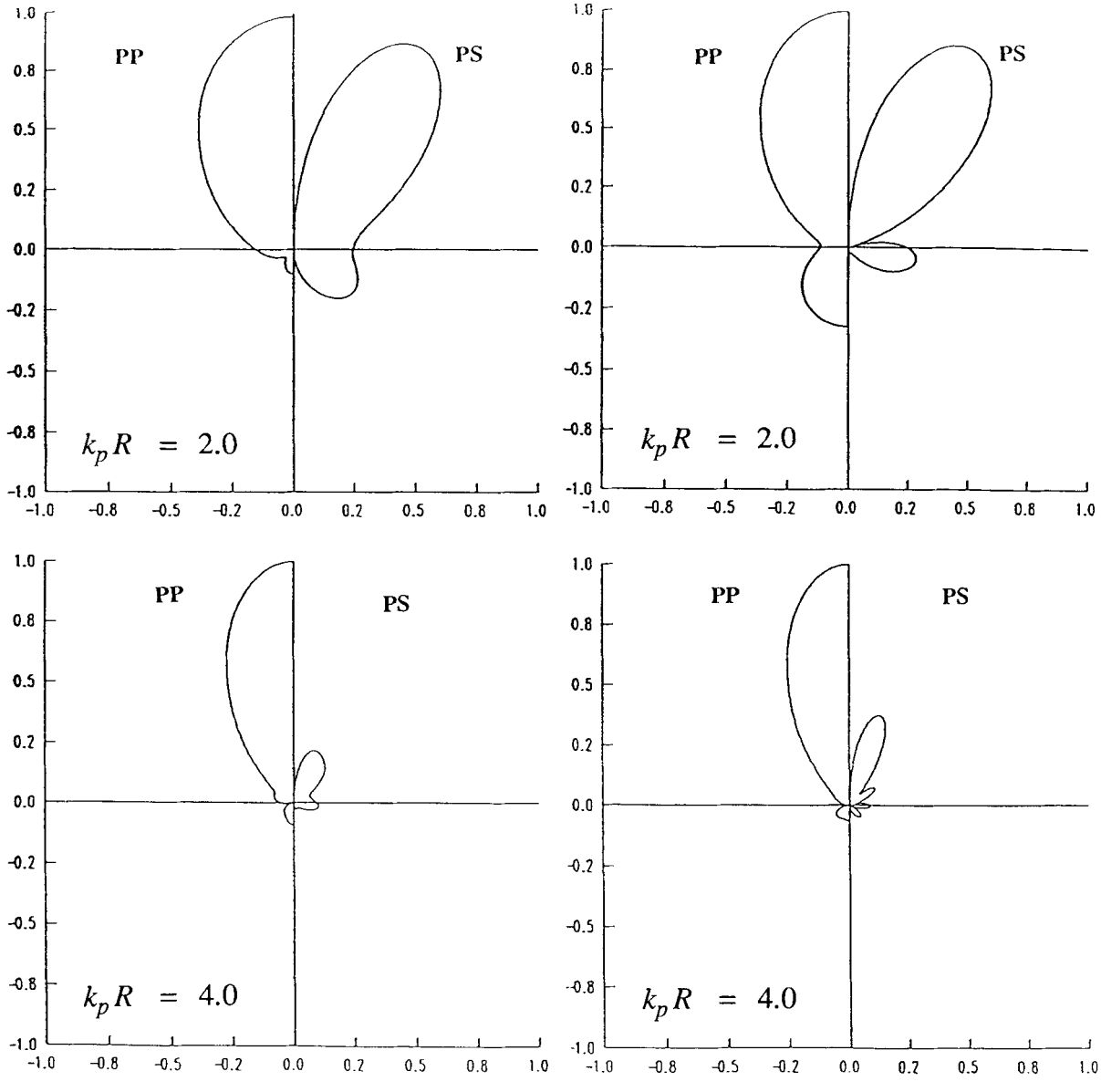

Figure 6(b). Similar to Fig. 6(a) except that the cases are for $k_pR = 2$ in the top two panels and for $k_pR = 4$ in the bottom two panels.

low-velocity inclusion and the high-velocity inclusion in Fig. 7. An interesting result shown here is that at low frequencies ($k_pR < 2$) more energy is scattered into the S field than into the P field, with the ratio reaching a factor of 2 or more in some ranges. At high frequencies (k_pR greater than about 5), the scattered energy flux is primarily in the P field. In this range the long large-amplitude oscillations are caused by interference between $P_2P_1P_2$ and $P_2\hat{P}_2P_2$ waves. The short small-amplitude oscillations that appear only for the case of the low-velocity sphere are caused by the focusing characteristic of a low-velocity inhomogeneity, essentially the waves multiply reflected within the sphere that are evident in Fig. 5.

In both the scattering diagrams of Fig. 6 and the scattering cross-sections of Fig. 7, the amplitudes of the scattered fields have been displayed, but information about their phases are not shown. It is important to remember that outside the sphere the total solution consists of the sum of the incident field $\mathbf{U}_0$ and the scattered field $\mathbf{U}_2$, and these two fields can add either constructively or destructively. From a physical viewpoint it is clear that when the primary field $\mathbf{U}_0$ interacts with the inclusion, it loses that part of its energy which is converted to scattered waves and this causes a change in the primary field. Thus, the additional field $\mathbf{U}_2$ must include both this change in the primary field as well as the secondary scattered waves. For instance, in the deep shadow where the total field is approximately zero, the field $\mathbf{U}_2$ must have a value that is close to $-\mathbf{U}_0$ in order to compensate for the primary field. Consequently, in the scattering diagrams of Fig. 6 the forward scattered P field approaches a value of 1 at high frequencies, but this is partly present in order to cancel the primary wave. In the case of the scattering cross sections of Fig. 7 this same phenomenon causes the scattered P field to approach an asymptotic value of approximately 2 at high frequencies. This follows from the fact that in this frequency range the scattered field consists of two basic terms, the energy necessary to cancel the primary field in the shadow and the energy which is scattered by the sphere, and by

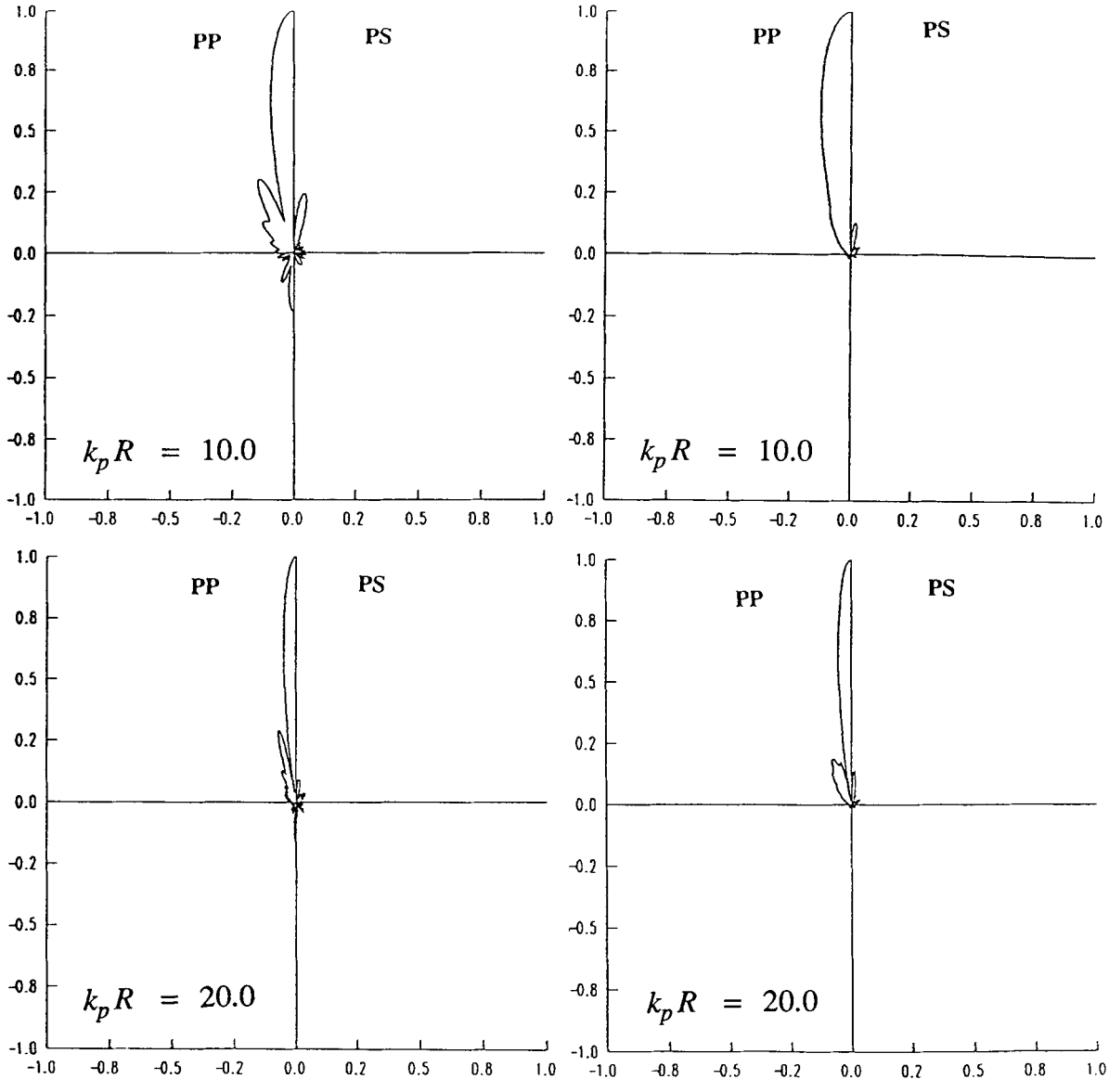

Figure 6(c). Similar to Fig. 6(a) except that the cases are for $k_pR = 10$ in the top two panels and for $k_pR = 20$ in the bottom two panels.

conservation of energy these two terms must be equal to each other and equal to the incident energy which is used to normalize the cross-sections. It helps in understanding this phenomenon to consider the case of a perfectly absorbing sphere, in which case there will not be any waves that are actually scattered, but the normalized scattering cross-sections will still have a value of 1.

6 CONCLUSIONS

The results presented in this paper can be used in a number of different ways. First, the complete and exact solution for the scattering of an elastic *P* wave by a spherical inclusion is presented in a convenient form. The various terms of the solution can be obtained either from the analytical solutions or a stable numerical procedure. Furthermore, a simple expression is developed for estimating the number of terms required in the harmonic series solution. The results are appropriate for arbitrary non-absorbing spherical inclusions, including fluids, and for all frequencies.

The numerical results calculated for the waves scattered from a spherical inclusion display a rich variety of interesting phenomena, some of which were briefly investigated in this study. In addition to the wavelength of the incident wave, the results depend critically upon the distance of the observation point from the scattering object. Within the shadow zone the waves which dominate the solution near the scatterer are quite different from those that dominate at larger distances. The solutions for low-velocity inclusions are quite different from those for high-velocity inclusions when near the scatterer, but these differences diminish at larger distances. Also, the solutions demonstrate that an inclusion can be quite effective in transforming incident *P* waves to scattered *S* waves, which may be important in the formation of seismic codas.

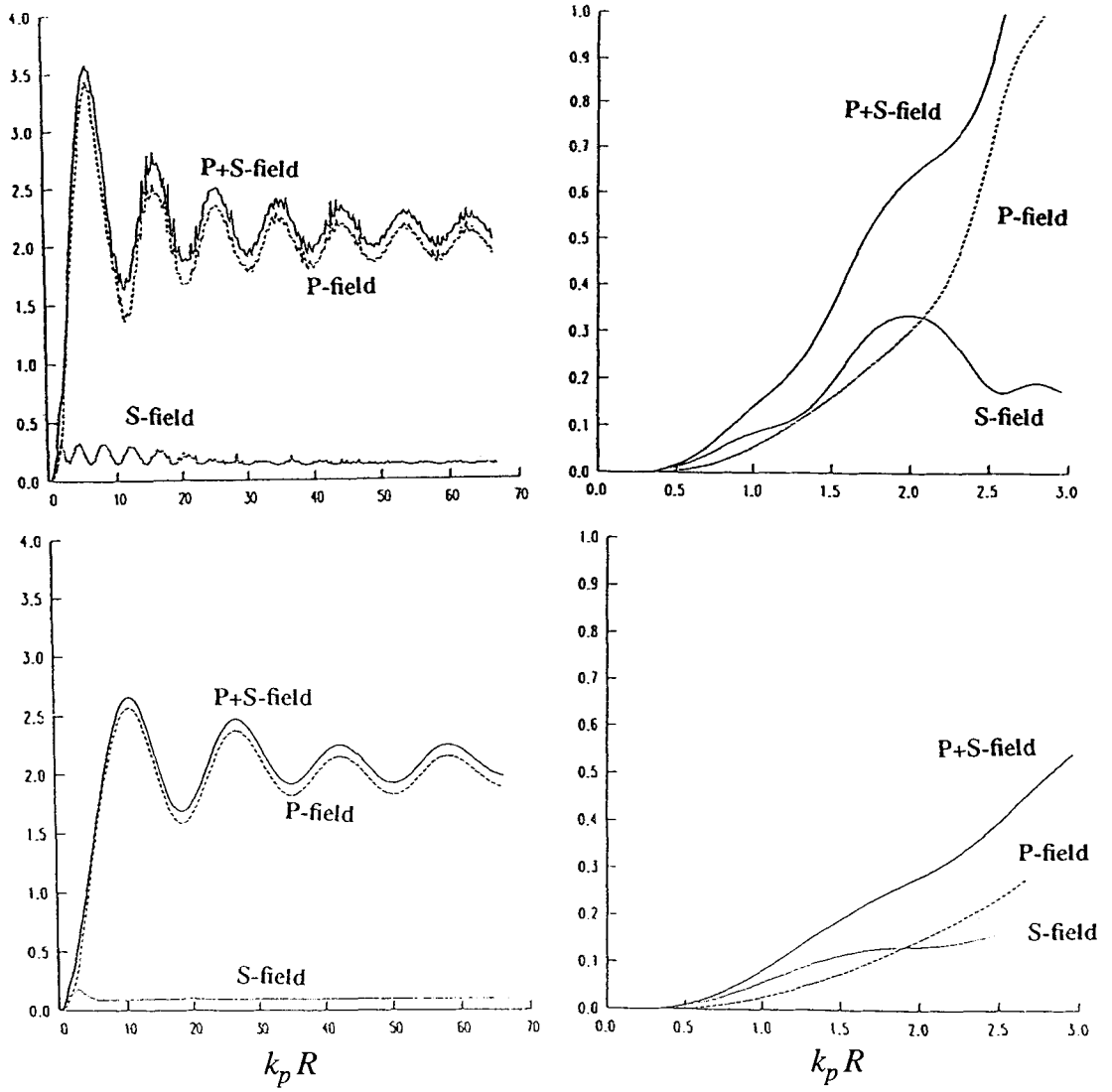

Figure 7. Normalized scattering cross-sections as a function of the parameter $k_pR = \omega R/V_p$. The top two panels are for model 1 of a low-velocity inclusion, and the bottom two panels are for model 2 of a high-velocity inclusion. The panels on the right are expanded versions of those on the left for small values of the argument.

The results presented in this paper should also be applicable, in at least an approximate manner, for problems involving scattering from heterogeneities more complicated than a simple sphere. Scattering by a sphere serves as a canonical problem for a general class of objects with relatively simple and smooth boundaries. It is expected that many of the scattering phenomena associated with the spherical inclusion will also apply to this wider class of heterogeneities.

Finally, as mentioned in the introduction, the results of this study can serve as the starting point for an investigation of various approximations that are typically made in the interpretation of scattered seismic waves. In assessing the validity of these approximations it is important to make comparisons with the exact solutions.

ACKNOWLEDGMENTS

One of the authors (VAK) gratefully acknowledges the guidance and assistance of Professor G. I. Petrashen in the development of the results that are presented in this paper. This research was supported by Phillips Laboratory under Contract F19628-90-K-0055 and also be the US Department of Energy under Contract DE-AC03-76SF00098.

REFERENCES

Aki, K., 1969. Analysis of the seismic coda of local earthquakes as scattered waves, *J. geophys. Res.*, **74,** 615–631.
Aki, K., 1973. Scattering of *P*-waves under the Montana LASA, *J. geophys. Res.*, **79,** 1334–1346.
Aki, K., 1980. Scattering and attenuation of shear waves in the lithosphere, *J. geophys. Res.*, **85,** 6469–6504.
Aki, K. & Richards, P. G., 1980. *Quantitative Seismology*, W. H. Freeman, New York.

Buldyrev, V. S., 1964. Diffraction of waves by a transparent sphere, Numerical methods of solution of differential and integral equations and integral formulas, in *Scientific Papers of Leningrad State University, Series in Mathematical Sciences,* pp. 287–291, (in Russian).
Buldyrev, V. S. & Molotkov, I. A., 1958. About the unharmonic propagation of waves in homogeneous and isotropic media with cylindrical and spherical boundaries, *Scientific Papers of Leningrad State University, Series in Mathematical Sciences,* **246,** 261–321, (in Russian).
Buldyrev, V. S. & Molotkov, I. A., 1960. Investigation of exact solutions of unharmonic diffraction problems near the wavefronts of slide waves, *Doklady Acad. Nauk USSR,* **134,** 1051–1054, (in Russian).
Clebsch, A., 1863. Uber die reflexion an einer kugelflache, *Crelle's J. Reine Angew. Math.,* **61,** 195, (in German).
Einspruch, N. G., Witterholt, E. J. & Truell, R., 1960. Scattering of a plane transverse wave by a spherical obstacle in an elastic medium, *J. appl. Phys.,* **31,** 806–818.
Gelchinskij, B. J., 1958. Some problems of wave propagation inside a homogeneous isotropic elastic sphere, *Scientific Papers of Leningrad State University, Series in Mathematical Sciences,* **246,** 322–345, (In Russian).
Gubernatis, J. E., Domany, E. & Krumhansl, J. A., 1977a. Formal aspects of the theory of the scattering of ultrasound by flaws in elastic materials, *J. appl. Phys.,* **48,** 2804–2811.
Gubernatis, J. E., Domany, E., Krumhansl, J. A. & Huberman, M., 1977b. The Born approximation in the theory of the scattering of elastic waves by flaws, *J. appl. Phys.,* **48,** 2812–2819.
Haddon, R. A. & Cleary, J. R., 1974. Evidence for scattering of seismic *PKP* waves near the mantle–core boundary. *Phys. Earth planet. Inter.,* **8,** 211–234.
Hudson, J. A., 1977. Scattered waves in the coda of *P, J. Geophys.,* **43,** 359–374.
Hudson, J. A. & Heritage, J. R., 1981. The use of the Born approximation in seismic scattering problems, *Geophys. J. R. astr. Soc.,* **66,** 221–240.
Korneev, V. A., 1983. About the calculation of eigenfrequencies of a radially-inhomogeneous elastic sphere, in *Problems of dynamic theory of seismic wave propagation,* **23,** 26–44, (in Russian), Nauka, Leningrad.
Korneev, V. A. & Johnson, L. R., 1993. Scattering of elastic waves by a spherical inclusion—II. Limitations of asymptotic solutions, *Geophys. J. Int.,* **115,** 251–263, (this issue).
Korneev, V. A. & Petrashen, G. I., 1987. Calculation of diffraction wave fields formed on an elastic sphere, in *Problems of dynamic theory of seismic wave propagation,* **27,** 26–44, (in Russian), Nauka, Leningrad.
Ludwig, D., 1970. Diffraction by a circular cavity, *J. math. Phys.,* **11,** 1617–1630.
Miles, J. W., 1960. Scattering of elastic waves by small inhomogeneities, *Geophysics,* **15,** 642–648.
Morse, P. M. & Feshbach, H., 1953. *Methods of Theoretical Physics,* McGraw-Hill, New York.
Nigul, U. K. *et al.* 1974. *Echo-signals from elastic objects. Part 2,* Academy of Science of Estonian SSR, Tallinn, (in Russian).
Nussenzveig, H. M., 1965. High-frequency scattering by an impenetrable sphere, *Ann. Phys.,* **34,** 23–95.
Nussenzveig, H. M., 1969. High-frequency scattering by a transparent sphere. I. Direct reflection and transmission, *J. math. Phys.,* **10,** 82–124.
Pao, Y.-H. & Mow, C. C., 1973. *Diffraction of Elastic Waves and Dynamic Stress Concentrations,* Crane Russak, New York.
Petrashen, G. I., 1945. Solution of vector boundary problems of mathematical physics in the case of a sphere, *Doklady Acad. Nauk USSR,* **46,** No. 7, (in Russian).
Petrashen, G. I., 1949. Symmetry of rotation and spherical vectors, *Scientific Papers of Leningrad State University, Series in Mathematical Sciences,* **114,** 3–27, (in Russian).
Petrashen, G. I., 1950. Dynamic problem of the theory of elasticity in the case of an isotropic sphere, *Scientific Papers of Leningrad State University, Series in Mathematical Sciences,* **135,** 24–70, (in Russian).
Rayleigh, Lord, 1871, On the scattering of light by small particles, *Phil. Mag.,* **41,** 447.
Scholte, J. G. J., 1956. On seismic waves in a spherical earth, *Koninkl. Med. Meteorol. Inst. Publ.,* **65,** 1–55.
Truell, R., Elbaum, C. & Chick, B. B., 1969. *Ultrasonic Methods in Solid State Physics,* Academic Press, New York.
Van der Hulst, H. C., 1957. *Light Scattering by Small Particles,* Wiley, New York.
Überall, H., 1973. Surface waves in acoustics, in *Physical Acoustics,* Vol. 10. pp. 1–60, eds Mason, W. P. & Thurston, R. N., Academic Press, New York.
Varatharajulu, V. & Pao, Y.-H., 1976. Scattering matrix for elastic waves. I. Theory, *J. acoust. Soc. Am.,* **60,** 556–566.
Watermann, P. C., 1976. Matrix theory of elastic wave scattering. *J. acoust. Soc. Am.,* **60,** 567–580.
Yamakawa, N., 1962. Scattering and attenuation of elastic waves, *Geophys. Mag.,* **31,** 63–103.
Ying, C. F. & Truell, R., 1956. Scattering of a plane longitudinal wave by a spherical obstacle in an isotropically elastic solid, *J. appl. Phys.,* **27,** 1086–1097.

APPENDIX A. SPHERICAL VECTOR SYSTEM

The spherical vector system used in this paper and its application to the problems of elastodynamics were developed by G. I. Petrashen. His original papers were published many years ago in Russian and are not readily available today. Thus we have included a brief summary of the system and its main properties in this appendix. More information can be found in Petrashen (1945, 1949) and Korneev & Petrashen (1987).

In a spherical coordinate system $\{r, \theta, \phi\}$ with unit vectors $(\hat{\mathbf{r}}, \hat{\boldsymbol{\theta}}, \hat{\boldsymbol{\phi}})$ the spherical vectors are defined by the expressions

$$\mathbf{Y}^{0}_{lm} \equiv \mathbf{Y}^{0}_{lm}(\theta, \phi) = \mathbf{r} \times \nabla Y_{lm}(\theta, \phi)$$

$$\mathbf{Y}^{+}_{lm} \equiv \mathbf{Y}^{+}_{lm}(\theta, \phi) = (l+1)\hat{\mathbf{r}} Y_{lm}(\theta, \phi) - r\,\nabla Y_{lm}(\theta, \phi) \qquad \text{(A1)}$$

$$\mathbf{Y}^{-}_{lm} \equiv \mathbf{Y}^{-}_{lm}(\theta, \phi) = l\hat{\mathbf{r}} Y_{lm}(\theta, \phi) + r\,\nabla Y_{lm}(\theta, \phi)$$

with the usual spherical harmonics

$$Y_{lm}(\theta, \phi) = e^{im\phi} P_l^m(\cos\theta), \qquad l \geq 0, \qquad -l \leq m \leq l$$

where $P_l^m(x)$ are the associated Legendre functions

$$P_l^m(x) = (1 - x^2)^{m/2} \frac{d^{l+m}}{dx^{l+m}} \frac{(x^2-1)^l}{2^l l!}, \qquad (m \geq 0)$$

$$P_l^m(x) = (-1)^{|m|} \frac{(l-|m|)!}{(l+|m|)!} P_l^{|m|}(x), \qquad (m < 0).$$

In a spherical coordinate system these vectors have the components

$$\mathbf{Y}_{lm}^0 = \frac{\partial Y_{lm}}{\partial\theta}\hat{\boldsymbol{\phi}} - \frac{1}{\sin\theta}\frac{\partial Y_{lm}}{\partial\phi}\hat{\boldsymbol{\theta}}$$

$$\mathbf{Y}_{lm}^+ = (l+1)Y_{lm}\hat{\mathbf{r}} - \frac{\partial Y_{lm}}{\partial\theta}\hat{\boldsymbol{\theta}} - \frac{1}{\sin\theta}\frac{\partial Y_{lm}}{\partial\phi}\hat{\boldsymbol{\phi}} \tag{A2}$$

$$\mathbf{Y}_{lm}^- = lY_{lm}\hat{\mathbf{r}} + \frac{\partial Y_{lm}}{\partial\theta}\hat{\boldsymbol{\theta}} + \frac{1}{\sin\theta}\frac{\partial Y_{lm}}{\partial\phi}\hat{\boldsymbol{\phi}}.$$

In a Cartesian coordinate system the components are

$$\begin{aligned}
\mathbf{Y}_{lm}^0 &= \frac{1}{2i}[Y_{l,m+1} + (l+m)(l-m+1)Y_{l,m-1}]\hat{\mathbf{x}} \\
&\quad - \tfrac{1}{2}[Y_{l,m+1} - (l+m)(l-m+1)Y_{l,m-1}]\hat{\mathbf{y}} + imY_{l,m}\hat{\mathbf{z}} \\
\mathbf{Y}_{lm}^+ &= \tfrac{1}{2}[Y_{l+1,m+1} - (l-m+1)(l-m+2)Y_{l+1,m-1}]\hat{\mathbf{x}} \\
&\quad + \frac{1}{2i}[Y_{l+1,m+1} + (l-m+1)(l-m+2)Y_{l+1,m-1}]\hat{\mathbf{y}} + (l-m+1)Y_{l+1,m}\hat{\mathbf{z}} \\
\mathbf{Y}_{lm}^- &= -\tfrac{1}{2}[Y_{l-1,m+1} - (l+m)(l+m-1)Y_{l-1,m-1}]\hat{\mathbf{x}} \\
&\quad - \frac{1}{2i}[Y_{l-1,m+1} + (l+m)(l+m-1)Y_{l-1,m-1}]\hat{\mathbf{y}} + (l+m)Y_{l-1,m}\hat{\mathbf{z}}.
\end{aligned} \tag{A3}$$

The spherical vectors of the system in eq. (A1) are linearly independent at any point (θ, ϕ) on a spherical surface. In the space of vector functions $\mathbf{f}(\theta, \phi)$ defined on a sphere Ω

$$0 \leq \theta \leq \pi, \qquad 0 \leq \phi \leq 2\pi, \qquad d\Omega = \sin\theta\, d\theta\, d\phi$$

the vectors satisfy the following orthogonality relation

$$\int_\Omega \mathbf{Y}_{lm}^{*(\nu)} \cdot \mathbf{Y}_{l_1 m_1}^{(\nu_1)}\, d\Omega = [c_{lm}^{(\nu)}]^{-2}\delta_{\nu\nu_1}\cdot\delta_{il_1}\cdot\delta_{mm_1} \tag{A4}$$

where the normalizing coefficients are given by the expressions

$$\begin{aligned}
c_{lm}^0 &= \sqrt{\frac{2l+1}{4\pi l(l+1)}\cdot\frac{(l-m)!}{(l+m)!}} \\
c_{lm}^+ &= \sqrt{\frac{1}{4\pi(l+1)}\cdot\frac{(l-m)!}{(l+m)!}} \\
c_{lm}^- &= \sqrt{\frac{1}{4\pi l}\cdot\frac{(l-m)!}{(l+m)!}}
\end{aligned} \tag{A5}$$

For vector functions $\mathbf{f}(\theta, \phi)$ with a finite norm

$$\int_\Omega |\mathbf{f}|^2\, d\Omega \equiv \int_\Omega \mathbf{f}^* \cdot \mathbf{f}\, d\Omega < \infty$$

the system of spherical vectors in eq. (A1) is complete in the sense of convergence in the mean for a generalized Fourier series expansion of $\mathbf{f}(\theta, \phi)$

$$\mathbf{f}(\theta, \phi) = \sum_{\nu=0,+,-} \sum_{l=0}^{\infty} \sum_{m=-l}^{l} a_{lm}^{(\nu)} \mathbf{Y}_{lm}^{(\nu)}(\theta, \phi) \tag{A6}$$

where

$$a_{lm}^{(\nu)} = [c_{lm}^{(\nu)}]^2 \int_{\Omega} \mathbf{Y}_{lm}^{*(\nu)} \cdot \mathbf{f}\, d\Omega. \tag{A7}$$

If the class of functions $\mathbf{f}(\theta, \phi)$ possesses continuous first derivatives with respect to θ and ϕ on the sphere Ω, then the series in eq. (A6) convergences uniformly and also possesses first derivatives with respect to θ and ϕ that agree with those of the original function.

The main feature of the spherical vectors of eq. (A1) is contained in their complete utilization of central symmetry when acted upon by any differential operator that is invariant to rotation. Consider an arbitrary differential operator $L(r, \theta, \phi)$ which is invariant to rotation of the spherical coordinate system (r, θ, ϕ). By invariant to rotation we mean that the operator L commutes with any other operator R that represents a rotation in 3-D space. Then, for an arbitrary function $\psi(r)$, possessing sufficient derivatives, we have the equality

$$L(r, \theta, \phi)[\psi(r)\mathbf{Y}_{lm}^{(\nu)}(\theta, \phi)] = [M_{lm}^{(\nu)}\psi(r)]\mathbf{Y}_{lm}^{(\nu)}(\theta, \phi), \qquad \nu = (0, +, -) \tag{A8}$$

where $M_{lm}^{(\nu)}(r)$ is an operator that acts on the radial function $\psi(r)$ only. This property together with the orthogonality relation in eq. (A4) means that for a differential equation of the form

$$L(r, \theta, \phi)\mathbf{U} = 0$$

substituting an expansion of the form

$$\mathbf{U} = \sum_{\nu,l,m} \psi_{lm}^{(\nu)}(r)\mathbf{Y}_{lm}^{(\nu)}(\theta, \phi)$$

converts the original system into a set of independent equations

$$M_{lm}^{(\nu)}\psi_{lm}^{(\nu)}(r) = 0$$

that only involve the radial functions $\psi_{lm}^{(\nu)}(r)$.

In many practical applications, it is necessary to know how the vector

$$\mathbf{U}_{lm} = \psi_{lm}^{0}(r)\mathbf{Y}_{lm}^{0} + \psi_{lm}^{+}(r)\mathbf{Y}_{lm}^{+} + \psi_{lm}^{-}(r)\mathbf{Y}_{lm}^{-}, \tag{A9}$$

responds to the following differential operators:

$$\nabla \cdot \mathbf{U}_{lm} = \left\{(l+1)\left[\psi_{lm,r}^{+} + \frac{(l+2)}{r}\psi_{lm}^{+}\right] + l\left[\psi_{lm,r}^{-} - \frac{(l-1)}{r}\psi_{lm}^{-}\right]\right\} Y_{lm}(\theta, \phi). \tag{A10}$$

$$\begin{aligned}\nabla \times \mathbf{U}_{lm} = {} & \left[\psi_{lm,r}^{-} - \frac{(l-1)}{r}\psi_{lm}^{-} - \psi_{lm,r}^{+} - \frac{(l+2)}{r}\psi_{lm}^{+}\right]\mathbf{Y}_{lm}^{0}(\theta, \phi) \\ & + \frac{l}{2l+1}\left[\psi_{lm,r}^{0} - \frac{l}{r}\psi_{lm}^{0}\right]\mathbf{Y}_{lm}^{+}(\theta, \phi) - \frac{l+1}{2l+1}\left[\psi_{lm,r}^{0} + \frac{l+1}{r}\psi_{lm}^{0}\right]\mathbf{Y}_{lm}^{-}(\theta, \phi).\end{aligned} \tag{A11}$$

$$\begin{aligned}\nabla^2\mathbf{U}_{lm} = {} & \left[(l+1)\left(\psi_{lm,rr}^{+} + \frac{2}{r}\psi_{lm,r}^{+} - \frac{(l+1)(l+2)}{r^2}\psi_{lm}^{+}\right)\right. \\ & \left. + l\left(\psi_{lm,rr}^{-} - \frac{(2l-1)}{r}\psi_{lm,r}^{-} + \frac{(l-1)(l+1)}{r^2}\psi_{lm}^{-}\right)\right]\frac{\mathbf{Y}_{lm}^{+}(\theta, \phi)}{2l+1} \\ & + \left[(l+1)\left(\psi_{lm,rr}^{+} + \frac{(2l+3)}{r}\psi_{lm,r}^{+} + \frac{l(l+2)}{r^2}\psi_{lm}^{+}\right)\right. \\ & \left. + l\left(\psi_{lm,rr}^{-} + \frac{2}{r}\psi_{lm,r}^{-} - \frac{l(l-1)}{r^2}\psi_{lm}^{-}\right)\right]\frac{\mathbf{Y}_{lm}^{-}(\theta, \phi)}{2l+1}.\end{aligned} \tag{A12}$$

$$\begin{aligned}\Delta\mathbf{U}_{lm} = \nabla^2\mathbf{U}_{lm} - \nabla \times \nabla \times \mathbf{U}_{lm} = {} & \left[\psi_{lm,rr}^{0} + \frac{2}{r}\psi_{lm,r}^{0} - \frac{l(l+1)}{r^2}\psi_{lm}^{0}\right]\mathbf{Y}_{lm}^{0}(\theta, \phi) \\ & + \left[\psi_{lm,rr}^{+} + \frac{2}{r}\psi_{lm,r}^{+} - \frac{(l+1)(l+2)}{r^2}\psi_{lm}^{+}\right]\mathbf{Y}_{lm}^{+}(\theta, \phi) \\ & + \left[\psi_{lm,rr}^{-} + \frac{2}{r}\psi_{lm,r}^{-} - \frac{l(l-1)}{r^2}\psi_{lm}^{-}\right]\mathbf{Y}_{lm}^{-}(\theta, \phi).\end{aligned} \tag{A13}$$

Finally we note that in the case of boundary conditions with cylindrical symmetry, it is convenient to use a cylindrical

vector system

$$\mathbf{Y}_m^0 = Y_m\hat{\mathbf{z}}$$
$$\mathbf{Y}_m^+ = Y_m\hat{\boldsymbol{\rho}} - iY_m\hat{\boldsymbol{\phi}} \tag{A14}$$
$$\mathbf{Y}_m^- = Y_m\hat{\boldsymbol{\rho}} + iY_m\hat{\boldsymbol{\phi}}$$

where $Y_m = e^{im\phi}$ and $(\hat{\boldsymbol{\rho}}, \hat{\boldsymbol{\phi}}, \hat{\mathbf{z}})$ are unit vectors of a cylindrical coordinate system (ρ, ϕ, z). For the case of cylindrical symmetry the vector system of eq. (A14) possesses the main features of the system of spherical vectors of eq. (A1).

APPENDIX B

The analytical solutions for the unknown coefficients in eq. (2.20) are

$$a_l^{(\nu)} = \frac{\Delta_a^{(\nu)}}{\Delta}, \qquad b_l^{(\nu)} = \frac{\Delta_b^{(\nu)}}{\Delta}, \qquad (\nu = 1, 2) \tag{B1}$$

where

$$\begin{aligned}\Delta = \frac{\eta_2\xi_2^3}{2l+1}\Bigg\{&\frac{h_l(\xi_2)}{\xi_2}\frac{h_l(\eta_2)}{\eta_2}(2l+1)\Delta_1 + \frac{j_l(\xi_1)}{\xi_1}\frac{j_l(\eta_1)}{\eta_1}(2l+1)\Delta_2\left(\frac{\rho_1}{\rho_2}\right)^2\\ &- (2l+1)\frac{\rho_1}{\rho_2}\left[\frac{h_l(\xi_2)}{\xi_2}\frac{j_l(\eta_1)}{\eta_1}\Delta_{12} + \frac{j_l(\xi_1)}{\xi_1}\frac{h_l(\eta_2)}{\eta_2}\Delta_{21}\right]\\ &- q\,\Delta_1[\Delta_2 + (l+2)h_{l+1}(\xi_2)h_{l+1}(\eta_2) + (l-1)h_{l-1}(\xi_2)h_{l-1}(\eta_2)]\\ &+ q\frac{\rho_1}{\rho_2}\Delta_2[\Delta_1 + (l+2)j_{l+1}(\xi_1)j_{l+1}(\eta_1) + (l-1)j_{l-1}(\xi_1)j_{l-1}(\eta_1)] + q^2(l-1)(l+2)\,\Delta_1\,\Delta_2\Bigg\}.\end{aligned} \tag{B2}$$

$$\begin{aligned}\Delta_a^{(1)} = i\eta_2^3\Bigg\{&\frac{h_l(\eta_2)}{\eta_2}\left[l\left(1 - \frac{\rho_1}{\rho_2} - (l+2)(2l+1)q\right)\frac{j_l(\eta_1)}{\eta_1} + (l(l+2)q - 1)j_{l-1}(\eta_1)\right]\\ &+ h_{l-1}(\eta_2)\left[\left(\frac{\rho_1}{\rho_2} + l(l+2)q\right)\frac{j_l(\eta_1)}{\eta_1} - qj_{l-1}(\eta_1)\right]\Bigg\}.\end{aligned} \tag{B3}$$

$$\begin{aligned}\Delta_b^{(1)} = -i\eta_2^3\Bigg\{&\frac{h_l(\eta_2)}{\eta_2}\left[\left(1 - \frac{\rho_1}{\rho_2} - (l+2)(2l+1)q\right)\frac{j_l(\xi_1)}{\xi_1} + (l+2)qj_{l-1}(\xi_1)\right]\\ &+ h_{l-1}(\eta_2)q\left[(l+2)\frac{j_l(\xi_1)}{\xi_1} - j_{l-1}(\xi_1)\right]\Bigg\}.\end{aligned} \tag{B4}$$

$$\begin{aligned}\Delta_b^{(2)} = i\eta_2^3\Bigg\{&j_{l-1}(\xi_1)j_{l-1}(\eta_1)q(1 - (l-1)(l+2)q) - \frac{j_l(\xi_1)}{\xi_1}\frac{j_l(\eta_1)}{\eta_1}\frac{\rho_1}{\rho_2}\left(1 - \frac{\rho_1}{\rho_2} - (l+2)(2l+1)q\right)\\ &+ j_{l-1}(\xi_1)\frac{j_l(\eta_1)}{\eta_1}q\left(l(l-1)(l+2)q - l - 2\frac{\rho_1}{\rho_2}\right) + j_{l-1}(\eta_1)\frac{j_l(\xi_1)}{\xi_1}q\left((l^2-1)(l+2)q - l - 1 - \frac{\rho_1}{\rho_2}\right)\Bigg\}.\end{aligned} \tag{B5}$$

The following relation exists between the terms in eqs (B3)–(B5).

$$\Delta_b^{(2)} = i\,\mathcal{I}m(\Delta_b^{(1)}\,\Delta_a^{(1)*}).$$

An expression for $\Delta_a^{(2)}$ can be derived from eq. (B2) by substituting for functions $h_k(\xi_2)$ $(k = l-1, l, l+1)$ the corresponding functions $-j_k(\xi_2)$. The following quantities were used in eqs (B2)–(B5)

$$\begin{aligned}\Delta_1 &= (l+1)j_{l+1}(\xi_1)j_{l-1}(\eta_1) + lj_{l-1}(\xi_1)j_{l+1}(\eta_1)\\ \Delta_2 &= (l+1)h_{l+1}(\xi_2)h_{l-1}(\eta_2) + lh_{l-1}(\xi_2)h_{l+1}(\eta_2)\\ \Delta_{12} &= (l+1)j_{l+1}(\xi_1)h_{l-1}(\eta_2) + lj_{l-1}(\xi_1)h_{l+1}(\eta_2)\\ \Delta_{21} &= (l+1)h_{l+1}(\xi_2)j_{l-1}(\eta_1) + lh_{l-1}(\xi_2)j_{l+1}(\eta_1)\end{aligned} \tag{B6}$$

$$q = \frac{2}{\eta_2^2}\left(1 - \frac{\rho_1\eta_2^2}{\rho_2\eta_1^2}\right) = \frac{2}{\eta_2^2}\left(1 - \frac{\mu_1}{\mu_2}\right).$$

For the case of a fluid within the sphere, the above equations can still be used provided the following substitutions are

made:

$$\mu_1 = 0, \qquad j_{l+1}(\eta_1) = 1, \qquad j_{l-1}(\eta_1) = -1, \qquad j_l(\eta_1) = 0. \tag{B7}$$

$$\begin{aligned}\Delta = \xi_2^3\Big\{&(2l+1)\frac{h_l(\xi_2)}{\xi_2}h_l(\eta_2)\Big(j_{l+1}(\xi_1) - \frac{l}{\xi_1}j_l(\xi_1)\Big)\\ &-(2l+1)\frac{\rho_1}{\rho_2}\frac{j_l(\xi_1)}{\xi_1}h_l(\eta_2)\Big(h_{l+1}(\xi_2) - \frac{l}{\xi_2}h_l(\xi_2)\Big)\\ &-\frac{2}{\eta_2}\Big(j_{l+1}(\xi_1) - \frac{l}{\xi_1}j_l(\xi_1)\Big)[\Delta_2 + (l+2)h_{l+1}(\xi_2)h_{l+1}(\eta_2) + (l-1)h_{l-1}(\xi_2)h_{l-1}(\eta_2)]\\ &+\frac{2}{\eta_2}\frac{\rho_1}{\rho_2}\Delta_2\Big(2j_{l+1}(\xi_1) - \frac{2l-1}{\xi_1}j_l(\xi_1)\Big) + \frac{4}{\eta_2^3}(l-1)(l+2)\,\Delta_2\Big(j_{l+1}(\xi_1) - \frac{l}{\xi_1}j_l(\xi_1)\Big)\Big\}.\end{aligned} \tag{B8}$$

$$\Delta_a^{(1)} = i\eta_2^2\Big\{h_l(\eta_2) + \frac{2}{\eta_2}\Big[(l^2-1)\frac{h_l(\eta_2)}{\eta_2} - h_{l+1}(\eta_2)\Big]\Big\}. \tag{B9}$$

$$\Delta_b^{(1)} = 0. \tag{B10}$$

$$\Delta_b^{(2)} = -2i\eta_2\Big\{j_{l-1}(\xi_1)(1-(l-1)(l+2)q) + \frac{j_l(\xi_1)}{\xi_1}\Big((l^2-1)(l+2)q - l - 1 - \frac{\rho_1}{\rho_2}\Big)\Big\}. \tag{B11}$$

An expression for $\Delta_a^{(2)}$ can be derived from the one for Δ in the same way as for the elastic case.